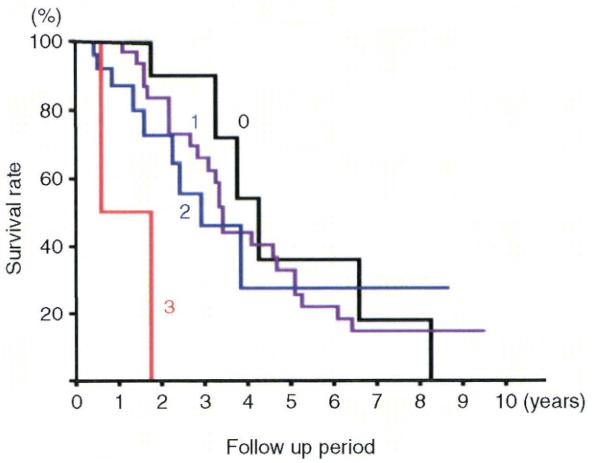

Figure 6 Overall survival according to Italian score (CLIP score) in 95 patients with grade I accumulation after chemoembolization.

changed, we recommend changing repeated chemoembolization using cisplatin and lipiodol when lipiodol accumulation is of grade II and III. That includes addition to ablation against the main tumor because of the limit on repeating chemoembolization, change of anticancer drug because of poor sensitivity and change of drug delivery such as hepatic arterial infusion chemotherapy without use of lipiodol[41–46] or recent developing molecular targeting therapy such as sorafenib.[47–49] In the future, which treatment strategy is better for those advanced HCC patients requires further investigations.

We could not conclude whether embolization is necessary for transcatheter chemoembolization in our study. Gelatin sponge embolization was not a significant prognostic factor in this study. Ikeda *et al.* also reported that although transarterial infusion chemotherapy with embolization had a stronger antitumor effect than transarterial infusion chemotherapy without embolization, it did not significantly improve survival.[17] In contrast, Yamamoto *et al.* reported that complete embolization after injection of cisplatin–lipiodol suspension resulted in higher survival than incomplete embolization.[50] We consider that gelatin sponge embolization was locally effective in the tumor, but because survival rates were also related to liver function, gelatin sponge embolization was not a significant prognostic factor in this study.

Our study had two important limitations. First, the study period was long, during which time remarkable advances in the diagnosis and treatment of HCC were achieved. Thus, the background characteristics of the patients were likely different. Nevertheless, in bias of treatment, we did restrict the study population to patients treated repeatedly with chemoembolization using cisplatin and lipiodol alone and analyzed the prognostic value of these staging systems. Moreover, we further restricted the population to 95 patients with grade I accumulation of lipiodol after first chemoembolization and analyzed the prognostic value of these staging systems. We therefore consider that any bias resulting from this extended study period would have been minimal in bias of treatment. Furthermore, in bias of diagnosis, chemoembolization was performed under DSA from 1983 to June 2000, and under CTAP and CTHA from June 2000 to December 2008. However, CT scan during hepatic arteriography and arterial portography (with vs without) were not predictors of survival by the log-rank test. We therefore consider that any bias resulting from this extended study period would have been minimal in bias of diagnosis, too.

Second, the sample size of the study was small, which may have limited our use of the AIC score. However, we omitted stage IV ($n = 5$) in TNM, score 3 ($n = 2$) in CLIP score, stage C ($n = 1$) and D ($n = 4$) in BCLC stage, score 0 ($n = 3$) and score 4 ($n = 3$) in JIS score, score 0 ($n = 4$), score 4 ($n = 1$) and score 5 ($n = 2$) in m-JIS due to small sample and re-analyzed by AIC score test. As a result, AIC score was in the descending order of modified-JIS (237.0), LCSGJ/TNM (248.3), JIS score (248.4), BCLC stage (255.5) and CLIP score (264.6). Therefore, we confirmed that the m-JIS system also had the best homogeneity ability.

In conclusion, this study shows that the discriminate ability of the m-JIS score is substantially better than that of the other staging systems and has better prognostic predictive power in patients with grade I accumulation of lipiodol after first chemoembolization.

REFERENCES

1 Okita K. Management of hepatocellular carcinoma in Japan. *J Gastroenterol* 2006; **41**: 100–6.
2 Taylor-Robinson SD, Foster GR, Arora S, Hargreaves S, Thomas HC. Increase in primary liver cancer in the UK, 1979–94. *Lancet* 1997; **350**: 1142–3.
3 El-Serag HB, Mason AC. Rising incidence of hepatocellular carcinoma in the United States. *N Engl J Med* 1999; **340**: 745–50.
4 El-Serag HB. Hepatocellular carcinoma: an epidemiologic view. *J Clin Gastroenterol* 2002; **35**: S72–8.
5 Kamangar F, Dores GM, Anderson WF. Patterns of cancer incidence, mortality, and prevalence across five continents:

defining priorities to reduce cancer disparities in different geographic regions of the world. *J Clin Oncol* 2006; **24**: 2137–50.
6 Livraghi T, Festi D, Monti F, Salmi A, Vettori C. US-guided percutaneous alcohol injection of small hepatic and abdominal tumors. *Radiology* 1986; **161**: 309–12.
7 Seki T, Wakabayashi M, Nakagawa T *et al.* Ultrasonically guided percutaneous microwave coagulation therapy for small hepatocellular carcinoma. *Cancer* 1994; **1**: 817–25.
8 Amin Z, Donald JJ, Masters A *et al.* Hepatic metastases: interstitial laser photocoagulation with real-time US monitoring and dynamic CT evaluation of treatment. *Radiology* 1993; **187**: 339–47.
9 Rossi S, Buscarini E, Garbagnati F *et al.* Percutaneous treatment of small hepatic tumors by an expandable RF needle electrode. *AJR Am J Roentgenol* 1998; **170**: 1015–22.
10 Buscarini L, Buscarini E, Di Stasi M, Vallisa D, Quaretti P, Rocca A. Percutaneous radiofrequency ablation of small hepatocellular carcinoma: long-term results. *Eur Radiol* 2001; **11**: 914–21.
11 Saneto H, Kobayashi M, Kawamura Y *et al.* Clinicopathological features, background liver disease, and survival analysis of HCV-positive patients with hepatocellular carcinoma: differences between young and elderly patients. *J Gastroenterol* 2008; **43**: 975–81.
12 Miki D, Aikata H, Uka K *et al.* Clinicopathological features of elderly patients with hepatitis C virus-related hepatocellular carcinoma. *J Gastroenterol* 2008; **43**: 550–7.
13 Noda I, Kitamoto M, Nakahara H *et al.* Regular surveillance by imaging for early detection and better prognosis of hepatocellular carcinoma in patients infected with hepatitis C virus. *J Gastroenterol* 2010; **5**: 105–12.
14 Yamada R, Sato M, Kawabata M, Nakatsuka H, Nakamura K, Takashima S. Hepatic artery embolization in 120 patients with unresectable hepatoma. *Radiology* 1983; **148**: 397–401.
15 Kamada K, Nakanishi T, Kitamoto M *et al.* Long-term prognosis of patients undergoing transcatheter arterial chemoembolization for unresectable hepatocellular carcinoma: comparison of cisplatin lipiodol suspension and doxorubicin hydrochloride emulsion. *J Vasc Interv Radiol* 2001; **12**: 847–54.
16 Kawaoka T, Aikata H, Takaki S *et al.* Transarterial infusion chemotherapy using cisplatin-lipiodol suspension with or without embolization for unresectable hepatocellular carcinoma. *Cardiovasc Intervent Radiol* 2009; **32**: 687–94.
17 Ikeda M, Maeda S, Shibata J *et al.* Transcatheter arterial chemotherapy with and without embolization in patients with hepatocellular carcinoma. *Oncology* 2004; **66**: 24–31.
18 Llovet JM, Real MI, Montana X *et al.* Arterial embolisation or chemoembolisation versus symptomatic treatment in patients with unresectable hepatocellular carcinoma: a randomised controlled trial. *Lancet* 2002; **18** (359): 1734–9.
19 Lo CM, Ngan H, Tso WK *et al.* Randomized controlled trial of transarterial lipiodol chemoembolization for unresectable hepatocellular carcinoma. *Hepatology* 2002; **35**: 1164–71.
20 Bruix J, Llovet JM, Castells A *et al.* Transarterial embolization versus symptomatic treatment in patients with advanced hepatocellular carcinoma: results of a randomized, controlled trial in a single institution. *Hepatology* 1998; **27**: 1578–83.
21 Pelletier G, Ducreux M, Gay F *et al.* Treatment of unresectable hepatocellular carcinoma with lipiodol chemoembolization: a multicenter randomized trial. Groupe CHC. *J Hepatol* 1998; **29**: 129–34.
22 Llovet JM, Bruix J. Systematic review of randomized trials for unresectable hepatocellular carcinoma: chemoembolization improves survival. *Hepatology* 2003; **37**: 429–42.
23 Bruix J, Sala M, Llovet JM. Chemoembolization for hepatocellular carcinoma. *Gastroenterology* 2004; **127**: S179–88.
24 The general rules for the clinical and pathological study of primary liver cancer. Liver Cancer Study Group of Japan. *Jpn J Surg* 1989; **19**: 98–129.
25 Kudo M, Chung H, Osaki Y. Prognostic staging system for hepatocellular carcinoma (CLIP score): its value and limitations, and a proposal for a new staging system, the Japan Integrated Staging Score (JIS score). *J Gastroenterol* 2003; **38**: 207–15.
26 A new prognostic system for hepatocellular carcinoma: a retrospective study of 435 patients: the Cancer of the Liver Italian Program (CLIP) investigators. *Hepatology* 1998; **28**: 751–5.
27 Llovet JM, Bru C, Bruix J. Prognosis of hepatocellular carcinoma: the BCLC staging classification. *Semin Liver Dis* 1999; **19**: 329–38.
28 Nanashima A, Sumida Y, Morino S *et al.* The Japanese integrated staging score using liver damage grade for hepatocellular carcinoma in patients after hepatectomy. *Eur J Surg Oncol* 2004; **30**: 765–70.
29 Yen YH, Changchien CS, Wang JH *et al.* A modified TNM-based Japan Integrated Score combined with AFP level may serve as a better staging system for early-stage predominant hepatocellular carcinoma patients. *Dig Liver Dis* 2009; **41**: 431–41.
30 Guglielmi A, Ruzzenente A, Pachera S *et al.* Comparison of seven staging systems in cirrhotic patients with hepatocellular carcinoma in a cohort of patients who underwent radiofrequency ablation with complete response. *Am J Gastroenterol* 2008; **103**: 597–604.
31 Huo TI, Lin HC, Hsia CY *et al.* The model for end-stage liver disease based cancer staging systems are better prognostic models for hepatocellular carcinoma: a prospective sequential survey. *Am J Gastroenterol* 2007; **102**: 1920–30.
32 Luo KZ, Itamoto T, Amano H *et al.* Comparative study of the Japan Integrated Stage (JIS) and modified JIS score as a predictor of survival after hepatectomy for hepatocellular carcinoma. *J Gastroenterol* 2008; **43**: 369–77.
33 Testa R, Testa E, Giannini E *et al.* Trans-catheter arterial chemoembolisation for hepatocellular carcinoma in

patients with viral cirrhosis: role of combined staging systems, Cancer Liver Italian Program (CLIP) and Model for End-stage Liver Disease (MELD), in predicting outcome after treatment. *Aliment Pharmacol Ther* 2003; **15**: 1563–9.
34 Kim JH, Choi JH, Kim CH *et al.* Value of the model for end-stage liver disease for predicting survival in hepatocellular carcinoma patients treated with transarterial chemoembolization. *Scand J Gastroenterol* 2009; **44**: 346–57.
35 Chuang VP, Wallace S. Hepatic artery embolization in the treatment of hepatic neoplasms. *Radiology* 1981; **140**: 51–8.
36 Ohishi H, Uchida H, Yoshimura H *et al.* Hepatocellular carcinoma detected by iodized oil. Use of anticancer agents. *Radiology* 1985; **154**: 25–9.
37 Nakamura H, Hashimoto T, Oi H, Sawada S. Transcatheter oily chemoembolization of hepatocellular carcinoma. *Radiology* 1989; **170**: 783–6.
38 Takayasu K, Arii S, Matsuo N *et al.* Comparison of CT findings with resected specimens after chemoembolization with iodized oil for hepatocellular carcinoma. *AJR Am J Roentgenol* 2000; **175**: 699–704.
39 Omagari K, Ohba K, Kadokawa Y *et al.* Comparison of the grade evaluated by "Liver damage" of Liver Cancer Study Group of Japan and Child-Pugh classification in patients with hepatocellular carcinoma. *Hepatol Res* 2006; **34**: 266–72.
40 Toyoda H, Kumada T, Kiriyama S *et al.* Comparison of the usefulness of three staging systems for hepatocellular carcinoma (CLIP, BCLC, and JIS) in Japan. *Am J Gastroenterol* 2005; **100**: 1764–71.
41 Uka K, Aikata H, Takaki S *et al.* Similar effects of recombinant interferon-alpha-2b and natural interferon-alpha when combined with intra-arterial 5-fluorouracil for the treatment of advanced hepatocellular carcinoma. *Liver Int* 2007; **27**: 1209–16.
42 Uka K, Aikata H, Takaki S *et al.* Pretreatment predictor of response, time to progression, and survival to intraarterial 5-fluorouracil/interferon combination therapy in patients with advanced hepatocellular carcinoma. *J Gastroenterol* 2007; **42**: 845–53.
43 Urabe T, Kaneko S, Matsushita E, Unoura M, Kobayashi K. Clinical pilot study of intrahepatic arterial chemotherapy with methotrexate, 5-fluorouracil, cisplatin and subcutaneous interferon-alpha-2b for patients with locally advanced hepatocellular carcinoma. *Oncology* 1998; **55**: 39–47.
44 Sakon M, Nagano H, Dono K *et al.* Combined intraarterial 5-fluorouracil and subcutaneous interferon-alpha therapy for advanced hepatocellular carcinoma with tumor thrombi in the major portal branches. *Cancer* 2002; **15**: 435–42.
45 Ota H, Nagano H, Sakon M *et al.* Treatment of hepatocellular carcinoma with major portal vein thrombosis by combined therapy with subcutaneous interferon-alpha and intra-arterial 5-fluorouracil; role of type 1 interferon receptor expression. *Br J Cancer* 2005; **5**: 557–64.
46 Obi S, Yoshida H, Toune R *et al.* Combination therapy of intraarterial 5-fluorouracil and systemic interferon-alpha for advanced hepatocellular carcinoma with portal venous invasion. *Cancer* 2006; **1**: 1990–7.
47 Llovet JM, Ricci S, Mazzaferro V *et al.* Sorafenib in advanced hepatocellular carcinoma. *N Engl J Med* 2008; **24**): 378–90.
48 Cheng AL, Kang YK, Chen Z *et al.* Efficacy and safety of sorafenib in patients in the Asia-Pacific region with advanced hepatocellular carcinoma: a phase III randomised, double-blind, placebo-controlled trial. *Lancet Oncol* 2009; **10**: 25–34.
49 Rimassa L, Santoro A. Sorafenib therapy in advanced hepatocellular carcinoma: the SHARP trial. *Expert Rev Anticancer Ther* 2009; **9**: 739–45.
50 Yamamoto K, Shimizu T, Narabayashi I. Intraarterial infusion chemotherapy with lipiodol-CDDP suspension for hepatocellular carcinoma. *Cardiovasc Intervent Radiol* 2000; **23**: 26–39.

The American Journal of Pathology, Vol. 177, No. 2, August 2010

DOI: 10.2353/ajpath.2010.090430

Epithelial and Mesenchymal Cell Biology

Hepatic Hyperplasia Associated with Discordant Xenogeneic Parenchymal-Nonparenchymal Interactions in Human Hepatocyte-Repopulated Mice

Rie Utoh,*† Chise Tateno,*‡§ Miho Kataoka,* Asato Tachibana,*§ Norio Masumoto,*¶ Chihiro Yamasaki,*§ Takashi Shimada,§ Toshiyuki Itamoto,¶ Toshimasa Asahara,¶ and Katsutoshi Yoshizato*‡§‖**

From the Yoshizato Project, Cooperative Link of Unique Science and Technology for Economy Revitalization (CLUSTER), Hiroshima Prefectural Institute of Industrial Science and Technology, Hiroshima; the Institute of Advanced Biomedical Engineering and Science,† Tokyo Women's Medical University, Tokyo; the Hiroshima University Liver Project Research Center,‡ Hiroshima; PhoenixBio Co.,§ Hiroshima; the Department of Surgery,¶ Division of Frontier Medical Science, Graduate School of Biomedical Sciences, Hiroshima University, Hiroshima; Liver Research Center,‖ Osaka City University Graduate School of Medicine, Osaka; and the Department of Biological Science,** Developmental Biology Laboratory and Hiroshima University 21st Century COE Program for Advanced Radiation Casualty Medicine, Graduate School of Science, Hiroshima University, Hiroshima, Japan*

Liver mass is optimized in relation to body mass. Rat (r) and human (h) hepatocytes were transplanted into liver-injured immunodeficient mice and allowed to proliferate for 3 or 11 weeks, respectively, when the transplants stopped proliferating. Liver/body weight ratio was normal throughout in r-hepatocyte-bearing mice (r-hep-mice), but increased continuously in h-hepatocyte-bearing mice (h-hep-mice), until reaching approximately three times the normal m-liver size, which was considered to be hyperplasia of h-hepatocytes because there were no significant differences in cell size among host (mouse [m-]) and donor (r- and h-) hepatocytes. Transforming growth factor-β (TGF-β) type I receptor, TGF-β type II receptor, and activin A type IIA receptor mRNAs in proliferating r-hepatocytes of r-hep-mice were lower than in resting r-hepatocytes (normal levels) and increased to normal levels during the termination phase. Concomitantly, m-hepatic stellate cells began to express TGF-β proteins. In stark contrast, TGF-β type II receptor and activin A type IIA receptor mRNAs in h-hepatocytes remained low throughout and m-hepatic stellate cells did not express TGF-β in h-hep-mice. As expected, Smad2 and 3 translocated into nuclei in r-hep-mice but not in h-hep-mice. Histological analysis showed a paucity of m-stellate cells in h-hepatocyte colonies of h-hep-mouse liver. We conclude that m-stellate cells are able to normally interact with concordant r-hepatocytes but not with discordant h-hepatocytes, which seems to be at least partly responsible for the failure of the liver size optimization in h-hep-mice. ***(Am J Pathol 2010, 177:654–665; DOI: 10.2353/ajpath.2010.090430)***

Experiments using animal models with damaged livers have demonstrated the high replicative potential of hepatocytes. A transgenic (Tg) mouse carrying an albumin (Alb) enhancer/promoter-driven murine urokinase-type plasminogen activator (uPA) gene was created[1]; the liver of this mouse degenerates and increases hepatocyte growth factor production and induces the proliferation of normal hepatocytes.[2] When transplanted into the uPA-Tg mice, mouse (m) hepatocytes engrafted into the host liver and proliferated, eventually replacing the host hepatocytes with a replacement index (RI) of 80%,[3] where RI represents the ratio of the regions occupied by transplanted hepatocytes in the host liver). The offspring generated by crossing uPA-Tg mice with immunodeficient mice were used as hosts for the xenotransplantation of rat (r),[4] woodchuck,[5] and human (h) hepatocytes.[6–8]

We showed that the repopulation kinetics of r-hepatocytes in uPA/severe combined immunodeficiency (SCID) mice were different from those of h-hepatocytes.[9] Rat

Supported in part by Cooperative Link of Unique Science and Technology for Economy Revitalization (CLUSTER), Promotion of Science and Technology in Regional Areas, Ministry of Education, Culture, Sports, Science and Technology, Japan.

Accepted for publication March 30, 2010.

None of the authors declare any relevant financial relationships.

Address reprint requests to Katsutoshi Yoshizato, Ph.D., PhoenixBio Co., Ltd., 3-4-1 Kagamiyama, Higashihiroshima, Hiroshima 739-0046, Japan. E-mail: katsutoshi.yoshizato@phoenixbio.co.jp.

hepatocytes rapidly proliferated and completely repopulated the mouse liver, whereas h-hepatocytes proliferated slowly over a longer period, with RI = ~90%. However, the livers of mice bearing h-hepatocytes (h-hep-mice) became much larger than the normal mass of the host mouse liver as the RI increased, whereas their counterparts with r-hepatocytes (r-hep-mice) did not (unpublished data). The above result with h-hep-mice does not meet the empirical rule (liver size optimization rule) that liver size is determined by the size of an animal's body.[10] This rule says that livers from smaller animals transplanted to larger animals must increase in size, which has been demonstrated in dogs,[10] humans,[11] and rats.[12]

Transforming growth factor (TGF)-β[13,14] and activin[15] are potent inhibitors of hepatocyte proliferation. The initiation of TGF-β signaling requires binding to the TGF-β type II receptor (TGFBR2), a constitutively active serine-threonine kinase, which subsequently *trans*-phosphorylates TGF-β type I receptor (TGFBR1). Activated TGFBR1 phosphorylates the Smad family proteins, Smad2 and 3 (Smad2/3), which then complex with Smad4 and translocate into the nucleus.[16] Smad2/3 are also activated by activin and nodal receptors, members of the TGF-β superfamily.[17] After partial hepatectomy, TGF-β mRNA expression increased in nonparenchymal cells, and TGF-β seemed to function as an inhibitory paracrine factor to prevent uncontrolled hepatocyte growth.[18]

When hepatocyte-targeted TGFBR2-knockout (KO) mice were subjected to 70% partial hepatectomy, hepatocytes grew beyond the limit of the known liver/body weight ratio ($R_{L/B}$),[19] supporting the antiproliferative role of TGF-β signaling. However, a similar study with hepatocyte-targeted TGFBR2-KO mice showed no significant differences in $R_{L/B}$ between control and KO mice because of an alternative increase in signaling via activin A/activin A type IIA receptor (ACVR2A) and persistent Smad pathway activity.[20] Thus, the roles of TGF-β, activin, and their receptors in the regulation of liver mass remain to be further studied.

In the present study, we compared the repopulation processes of concordant (rat) and discordant (human) xenogeneic hepatocytes in the uPA/SCID mouse liver. Our results showed that r-hep-mice had normal mouse regulation of $R_{L/B}$, whereas h-hep-mice underwent liver hyperplasia, resulting in the increase in $R_{L/B}$. The present study strongly suggests that discordant h-hepatocytes fail in exchanging molecular signals including TGF-β/activin with m-hepatic stellate cell (HSCs) and proliferate over the liver size optimization rule for mouse.

Materials and Methods

Preparation of Liver Tissues and Hepatocytes

The Hiroshima Prefectural Institute of Industrial Science and Technology Ethics Board approved this study. Liver tissues were obtained from seven donors in hospitals, with informed consent before the operations in accordance with the 1975 Declaration of Helsinki: four males, a 12-year-old male (12YM), a 28-year-old male (28YM), a 49-year-old male (49YM), and a 50-year-old male (50YM), and three females, a 25-year-old female (25YF), a 61-year-old female (61YF), and a 65-year-old female (65YF). The livers from the 25YF, 28YM, and 61YF were used for real-time RT-PCR to determine the expression levels of cell cycle-related genes and TGFBR/ACVR genes, and those from the 49YM, 50YM, and 65YF were used for immunostaining of proteins. Liver tissues were resected from 13-week-old male Fischer 344 rats (Charles River, Yokohama, Japan) and were used for real-time RT-PCR to determine the expression levels and immunohistochemistry.

h-Hepatocytes were isolated from the 12YM as reported previously.[7,21] Cryopreserved h-hepatocytes from two males, a 9-month-old male (9MM) and a 13-year-old male (13YM), were obtained from In Vitro Technologies (Baltimore, MD); h-hepatocytes from a 10-year-old female (10YF) were purchased from BD Biosciences (San Jose, CA). The hepatocytes from these four donors were used for transplantation experiments into uPA/SCID mice. r-Hepatocytes were isolated from the livers of Fischer 344 rats by collagenase perfusion,[22] centrifuged through 45% Percoll at 50 × *g* for 24 minutes and used for transplantation experiments. These hepatocyte preparations all showed >80% of viability, which was determined by the dye extrusion test, and >99% of purity, which was determined by microscopic observation.

Transplantation of Hepatocytes

h- and r-Hepatocytes, 7.5×10^5 and 5×10^5 cells, respectively, were transplanted into the liver of homozygous uPA/SCID mice, which had been generated by crossing uPA-Tg mice with SCID mice.[7] Donor h-hepatocytes showed reproducibly high engraftment efficiency similar to fresh r-hepatocytes and RI >80% under the optimized conditions. The labeling index (LI) of 5-bromo-2′-deoxyuridine (BrdU) of the transplanted hepatocytes was determined as a measure of DNA synthesis by exposing the host animals to BrdU for 1 hour before sacrifice.[23]

Histochemistry

Paraffin and frozen sections of 5-μm thickness were prepared from liver tissues as detailed previously.[7,23] The sections were stained with H&E or subjected to immunohistochemical analysis using the primary antibodies listed in Table 1 together with necessary information. For bright-field immunohistochemistry, the antibodies were visualized with the VECTASTAIN ABC kit (Vector Laboratories, Burlingame, CA) using 3,3′-diaminobenzidine as the substrate. The sections were counterstained with Mayer's hematoxylin. Fluorescent immunohistochemistry was performed using Alexa 488- or 594-conjugated donkey anti-mouse IgG or donkey anti-rabbit IgG (Invitrogen) as secondary antibodies and then with Hoechst 33258 for nuclear staining. Human cytokeratin 8/18 (hCK8/18) antibodies reacted with h-hepatocytes but not with m-hepatocytes. Rat major histocompatability complex class I RT1A (rRT1A) antibodies reacted with r-hepatocytes but not with m-hepatocytes. The RIs of h- and r-hepatocytes ($RI_{h\text{-}hep}$ and $RI_{r\text{-}hep}$, respectively) were calculated as the ratios of the

Table 1. Antibodies for Immunohistochemical Analysis

Antibodies	Clone (clone name)	Host	Dilution	Fixation	Sections	Supplier
Human CK8/18*	Monoclonal (NCL 5D3)	Mouse	50	Aceton	Frozen	MP Biomedicals (Aurora, OH)
Human albumin* (cross-adsorbed)	Polyclonal	Goat	200	Formalin	Paraffin	Bethyl Laboratories (Montgomery, TX)
BrdU	Monoclonal (Bu20a)	Mouse	50	Formalin	Paraffin	DAKO (Glostrup, Denmark)
Rat RT1A†	Monoclonal (OX-18)	Mouse	100	Aceton	Frozen	Chemicon International (Temecula, CA)
Mouse type IV collagen	Polyclonal	Rabbit	500	Aceton	Frozen	LSL (Tokyo, Japan)
Human MRP2‡	Polyclonal	Rabbit	200	Aceton	Frozen	Sigma (St. Louis, MO)
Human TGFBR2§	Polyclonal	Rabbit	500	Aceton	Frozen	Upstate (Billerica, MA)
TGF-β1¶	Polyclonal	Rabbit	10	Formalin	Frozen	BioVision (Mountain View, CA)
Human desmin§	Monoclonal	Mouse	50	Formalin	Frozen	DAKO
Human Smad2§	Polyclonal	Rabbit	50	Non-fixed	Frozen	Zymed Laboratories (South San Francisco, CA)
Human Smad3§	Polyclonal	Rabbit	200	Formalin	Paraffin	Zymed Laboratories
Human E-cadherin§	Polyclonal	Rabbit	200	Formalin	Frozen	Abcam (Cambridge, MA)

*Human-specific antibody.
†Rat-specific antibody.
‡Cross-reactive with rat antigen.
§Cross-reactive with rat and mouse antigens.
¶Cross-reactive with TGF-β1-3.

area occupied by hCK8/18$^+$ h-hepatocytes and the area occupied by rRT1A$^+$ r-hepatocytes to the entire area examined on immunohistochemical sections from six lobes, respectively, as described previously.[7] BrdU LIs of h- and r-hepatocytes ($LI_{h\text{-}hep}$ and $LI_{r\text{-}hep}$, respectively) were calculated as the ratios of BrdU$^+$ nuclei to hAlb$^+$ h-hepatocytes and rRT1A$^+$ r-hepatocytes, respectively, in 10 randomly selected fields from three different lobes.

A transferase-mediated dUTP nick end-labeling (TUNEL) assay was performed as follows. Paraffin-embedded liver tissues were sectioned, deparaffinized, and subjected to TUNEL analysis using an ApopTag Peroxidase In Situ Apoptosis Detection Kit (Chemicon International, Temecula, CA) following the manufacturer's instructions.

Real-Time RT-PCR

Total RNA was isolated from normal and chimeric liver tissues using Isogen (Nippon Gene, Tokyo, Japan) and aliquots, 1 μg each, were reverse-transcribed with random hexamers using PowerScript Reverse Transcriptase (Clontech, Kyoto, Japan). The expressions of the following genes were measured by real-time RT-PCR using an SYBR Green PCR Master Mix (Applied Biosystems, Foster City, CA) in an ABI Prism 7700 sequence detector (Applied Biosystems): h-forkhead box M1 (hFoxM1), h-cyclin dependent kinases (hCdk) 1, hCyclin B1, hCyclin D1, h-cell division cycle 25A (hCdc25A), hTGFBR1, hTGFBR2, hACVR2A, h-glyceraldehyde 3-phosphate dehydrogenase (hGAPDH), rat TGFBR1 (rTGFBR1), rTGFBR2, rACVR2A, and rGAPDH. The gene-specific primers we used are shown in Table 2. These primers correctly amplified the corresponding human/rat genes but not the mouse genes. The relative mRNA expressions of transplanted h- and r-hepatocytes were quantified using the comparative threshold cycle ($\Delta\Delta C_T$) method[24] according to the manual provided by Applied Biosystems. hGAPDH and rGAPDH, respectively, were used as the internal reference genes to normalize the expression of human/

Table 2. Primer Sets for Real-Time RT-PCR

Gene	Forward primer	Reverse primer
hFoxM1	5′-GCATCTACTGCCTCCCTGTG-3′	5′-GAGGAGTCTGCTGGGAACG-3′
hCdk1	5′-AAACTACAGGTCAAGTGG-3′	5′-GGGATAGAATCCAAGTATTTCTTCAG-3′
hCyclin B1	5′-CCTGATGGAACTAACTATGTTG-3′	5′-CATGTGCTTTGTAAGTCCTTGA-3′
hCyclin D1	5′-TGTGAAGTTCATTTCCAATCCG-3′	5′-CTGGAGAGGAAGCGTGTGAG-3′
hCdc25A	5′-CAAAGAGGAGGAAGAGCATGTC-3′	5′-CCAGGGATAAAGACTGATGAAGAG-3′
hTGFBR1	5′-GGAATTCATGAAGATTACCAAC-3′	5′-AGAGTTCAGGCAAAGCTGTAGA-3′
hTGFBR2	5′-CATGTGTTCCTGTAGCTCTGAT-3′	5′-TGCCGGTTTCCCAGGTTGA-3′
hACVR2A	5′-AAGAAGACCCTTTGTTGAAAAATG-3′	5′-GCAAGGTTTCTCTTAGTCTCATGTC-3′
hSmad2	5′-AAAGCTTCACCAATCAAGTCC-3′	5′-CTTCTCTTCCTCTTTAATGGG-3′
hSmad3	5′-TGGAACTCTACTCAACCCAT-3′	5′-GGTAAATGTGTTTGGCAGAC-3′
hGAPDH	5′-ACCAGGGCTGCTTTTAACTC-3′	5′-ATTGATGACAAGCTTCCCG-3′
rTGFBR1	5′-CACTTCTGATTCCCACTCTTG-3′	5′-ATGAAGGAGCAGGAGCTGTA-3′
rTGFBR2	5′-CAAGTCGGTTAACAGCGAT-3′	5′-GGCTTCTCACAGATGGAGG-3′
rACVR2A	5′-AGCATGGATTGGGAGACTTC-3′	5′-GCCACATTCTTCGTGTAAGTT-3′
rGAPDH	5′-CCAGGGCTGCCTTCTCTTGTGA-3′	5′-GCCGTTGAACTTGCCGTGGGTA-3′

h, human-specific; r, rat-specific.

rat target genes; h/r-specific primers were used because there is a difference in the amounts of h/r-cDNAs in the mixed baths from the h- or r-hep-mouse liver. Before performing quantification with the $\Delta\Delta C_T$ method, we confirmed that the amplification efficiencies of target and reference primers were approximately equal. The expression levels of the target genes show the relative differences from the normal h/r-liver controls. For all data, the h/r target C_T value was normalized using the formula: $\Delta C_T = C_T$ h/r target $- C_T$ h/rGAPDH. To determine the relative expression levels, the formula, $\Delta\Delta C_T = \Delta C_T$ sample (chimeric livers) $- \Delta C_T$ calibrator (h/r-livers), was used and $2^{-\Delta\Delta C_T}$ was plotted.

Statistics

Results are shown as the mean ± SD. Significant differences between groups were detected with Dunnett's multiple comparison test or Student's *t*-tests using StatView software (SAS Institute Japan, Tokyo, Japan).

Results

Growth Kinetics for r- and h-Hepatocytes in uPA/SCID Mice

Twelve mice were transplanted with r-hepatocytes and sacrificed at 1, 2, 3, and 4 weeks after transplantation. Liver sections were subjected to double immunostaining for BrdU and rRT1A to determine the $LI_{r\text{-}hep}$ and the $RI_{r\text{-}hep}$ (Figure 1A), where $LI_{r\text{-}hep}$ represents the ratio of the BrdU-positive r-hepatocyte number to the total r-hepatocytes in the r-hepatocyte-repopulated region in the r-hep-mouse liver, and $RI_{r\text{-}hep}$ represents the ratio of the repopulated r-hepatocytes to the total r- and m-hepatocytes in the r-hep-mouse liver. $LI_{r\text{-}hep}$ was approximately 15% at 1 week, when $RI_{r\text{-}hep}$ was approximately 7%. $RI_{r\text{-}hep}$ reached almost 100% at 3 weeks when $LI_{r\text{-}hep}$ had markedly decreased to 1%. Finally, $LI_{r\text{-}hep}$ returned to the control level (0.4%) at 4 weeks, the level of LI of SCID mouse liver. From these results, we concluded that r-hepatocytes terminated proliferation at approximately 3 weeks.

Mice were transplanted with h-hepatocytes isolated from the 9MM ($h\text{-}hep_{9MM}$) and were sacrificed at 1 to 11 weeks after transplantation (Figure 1B). $LI_{h\text{-}hep}$ and $RI_{h\text{-}hep}$, the corresponding ratios for h-hep-mouse liver, were approximately 10% and <1% at 1 week, respectively. The $LI_{h\text{-}hep}$ at this time period was 64% of the $LI_{r\text{-}hep}$. The rise of $RI_{h\text{-}hep}$ and the decrease of $LI_{h\text{-}hep}$ thereafter were both greatly slow compared with those of the r-hep-mice. $LI_{h\text{-}hep}$ returned to the control level at 11 weeks when $RI_{h\text{-}hep}$ was still as low as 58 ± 46%. Thus, it was concluded that h-hepatocytes repopulate the m-liver quite slowly. We believe that this difference in donor proliferative and repopulating activities is due to species-related differences but not experimental variables that might influence transplantation outcomes, because, first, the engraftment efficiencies were similar between the h- and the r-hepatocytes, second, the viability (>80%) and the purity (>99%) of the hepatocyte preparations were comparable between the two types of hepatocytes, and, third, the similar difference was observed

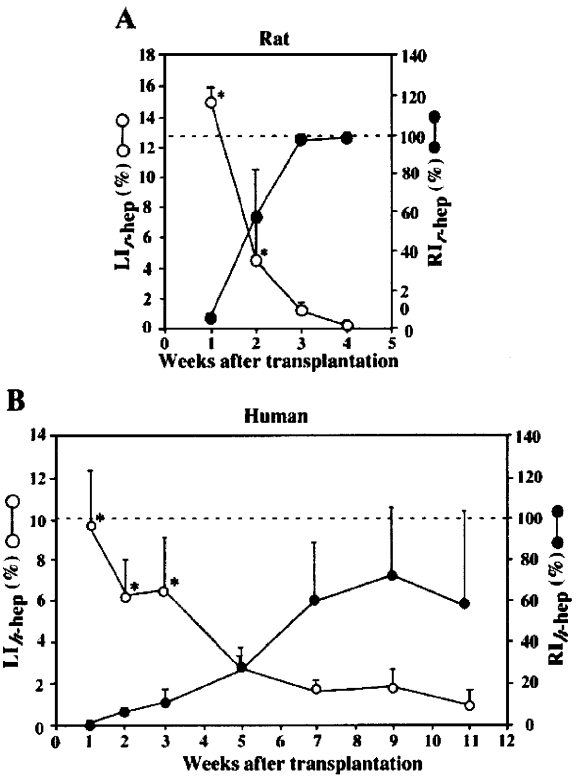

Figure 1. Repopulation of r- and h-hepatocytes in mice. uPA/SCID mice were transplanted with r-hepatocytes (**A**) and h-hepatocytes (**B**) and sacrificed at the indicated times (weeks) after transplantation. **A:** r-hep-Mice. Histological sections were prepared from three different lobes and stained for rRT1A and BrdU. $rRT1A^+$ and $BrdU^+$ double-positive hepatocytes and $rRT1A^+$ hepatocytes were counted to determine $LI_{r\text{-}hep}$ (open circle) and $RI_{r\text{-}hep}$ (closed circle), respectively. **B:** $h\text{-}hep_{9MM}$-Mice. $LI_{h\text{-}hep}$ (open circle) and $RI_{h\text{-}hep}$ (closed circle) were similarly determined, except that h-hepatocytes were identified using hAlb antibodies. The LI of livers taken from control animals (8- to 15-week-old SCID mice) was 0.4 ± 0.2% (n = 3). Significant differences compared with normal livers (*$P < 0.05$). The dotted horizontal line indicates RI = 100%.

in the previous report in which h-hepatocytes were also used as donor hepatocytes.[9]

Information regarding proliferative activity of h-hepatocytes was obtained by determining the gene expression levels of five cell cycle promotion genes (hCdk1, hCyclin B, hFoxM1, hCdc25A, and hCyclin D) in the h-hep-mouse livers during repopulation, together with those in normal h-livers from three donors. The results are shown as the relative mRNA expression levels against those in the normal h-livers (Figure 2). h-hep-Mouse livers expressed hCdk1 and hCyclin B1 at much and moderately higher levels at 3 to 9 weeks, respectively. The expressions of hFoxM1 and hCdc25A were significantly higher in h-hep-mouse livers up to 7 weeks. These genes all reduced the expression to levels comparative to normal h-liver levels at 11 weeks. These results indicate that h-hepatocytes in h-hep-mice terminated growth at 11 weeks after transplantation.

Correlation of $R_{L/B}$ with RI in h-Chimeric Mice

In the experiments shown in Figure 1, we noticed that the h-hep-mouse liver enlarged beyond the normal volume of

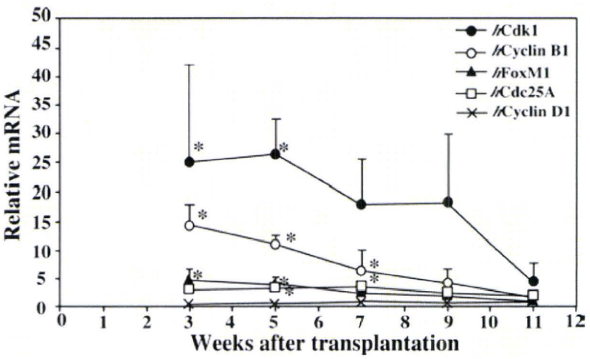

Figure 2. Expressions of cell cycle-related genes during h-hepatocyte repopulation in h-hep-mice. h-hep-Mouse livers were removed at 3 to 11 weeks after transplantation from h-hep-mice shown in Figure 1B and subjected to real-time RT-PCR for hCdk1 (closed circle), hCyclin B1 (open circle), hFoxM1 (closed triangle), hCdc25A (open square), and hCyclin D1 (×). Gene expressions were also determined for normal human livers from the 25YF, 28YM, and 61YF donors. Gene expressions were all normalized to hGAPDH expression. The ratio of mRNA expression for each gene in h-hep-mouse livers was calculated by dividing the normalized value of each gene of h-hep-mouse livers by the normalized value of corresponding gene of the normal h-livers. The ratios are plotted against weeks after transplantation. The variation of each gene of the normal livers was 1.0 ± 0.3, 1.0 ± 0.6, 1.0 ± 0.4, 1.0 ± 0.5, and 1.0 ± 0.3 for hFoxM1, hCdk1, hCyclin B1, hCyclin D1, and hCdc25A, respectively. Significant differences against normal h-livers (*$P < 0.05$).

the host liver as $RI_{h\text{-}hep}$ increased. We assessed a correlation between $RI_{h\text{-}hep}$ and liver mass during h-hepatocyte repopulation. A total of 38 h-hep-mice were generated using h-hepatocytes from three donors (9MM, 12YM, and 13YM) and were sacrificed at 11 to 14 weeks after transplantation. No significant increase in blood hAlb levels was observed at 9 to 10 weeks, indicating that the livers then had entered the termination phase of growth, which is consistent with the results shown in Figure 2. Host liver and body weights were measured at sacrifice to calculate $R_{L/B}$. Liver sections were prepared from each mouse and stained for hCK8/18 to determine RI. $R_{L/B}$ was then plotted against RI (Figure 3A). $R_{L/B}$ increased as RI increased, with a correlation coefficient (r^2) of 0.59. The gross appearances of the selected h-hep-mouse livers are shown in Figure 3, B–D. Livers of an h-hep-mouse with RI = 0% showed $R_{L/B}$ = 6.9 ± 1.0% (Figure 3, A and B). Twenty of the 38 h-hep-mice showed RI >50%. Five h-hep-mice showed RIs >80%, one of which had $R_{L/B}$ = 11.8% and is shown in Figure 3C. The highest RI was 92.1%, which was obtained in a chimeric $h\text{-}hep_{9MM}$ mouse with $R_{L/B}$ = 19.3% (Figure 3D). The $R_{L/B}$ for the five mice with RIs >80% was 13.2 ± 3.5%, which was >2-fold of the value at the time of transplantation (6.0 ± 1.1%, n = 4) or that (5.4 ± 0.5%, n = 3) observed in SCID mice (Figure 3A). Importantly, the $R_{L/B}$ of r-hep-mice did not change during repopulation (Figure 3E, 5 weeks) and was similar to that of SCID mice (5.4 ± 0.5%, n = 3): $R_{L/B}$ = 6.5 ± 1.1, 6.3 ± 0.2, 6.4 ± 0.2, and 5.8 ± 0.2% (each n = 3), at 2, 3, 4, and 5 weeks after transplantation, when RIs were 57.1 ± 24.7, 97.1 ± 3.0, 98.6 ± 2.4, and 100 ± 0.0%, respectively. This fact suggests that the increase in r-hepatocyte number and the death of injured m-hepatocytes are normally balanced in the r-hep-mouse liver. However, $R_{L/B}$ of h-hep-mice increased as the RI increased as above, suggesting a possible

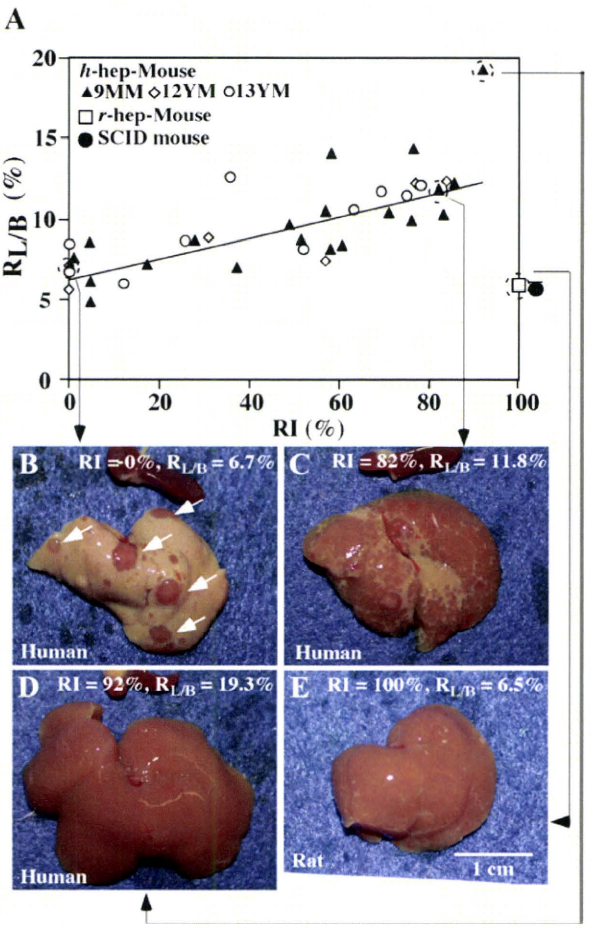

Figure 3. Correlation of $R_{L/B}$ with RI in h-hep-mice. **A:** Twenty-one, 6, and 11 h-hep-mice were produced by transplanting hepatocytes from the 9MM, 12YM, and 13YM donors, respectively, and then sacrificed at 11 to 14 weeks after transplantation. $R_{L/B}$ and RI were determined at sacrifice and plotted together. Closed triangle, 9MM hepatocytes; open diamond, 12YM hepatocytes; open circle, 13YM hepatocytes. Four r-hep-mice were produced and sacrificed at five weeks after transplantation when the repopulation had completed, and $R_{L/B}$ and RI were determined (open square). $R_{L/B}$ was also determined for three 8- to 15-week-old SCID mice (closed circle). **B–D:** Gross appearances of h-hep-mouse livers at 11 weeks. The four **long arrows** in the figure starting from each of mouse symbols in **A** point to the photos of the corresponding mouse livers shown in **B**, **C**, **D**, and **E**, respectively. **B:** The liver of an $h\text{-}hep_{9MM}$ mouse with RI = 0% and $R_{L/B}$ = 6.7%. **Arrows** indicate reddish colonies of m-hepatocytes that deleted the transgene. Whitish regions are occupied by Tg host hepatocytes. The dark red-colored organ placed above the liver is spleen removed from the same recipient. **C:** The liver of an $h\text{-}hep_{9MM}$ mouse with RI = 82% and $R_{L/B}$ = 11.8%. **D:** The liver of an $h\text{-}hep_{9MM}$ mouse with RI = 92% and $R_{L/B}$ = 19.3%. **E:** The liver of an r-hep-mouse with RI = 100% and $R_{L/B}$ = 6.5%. Scale bar = 1 cm.

imbalance between h-hepatocyte proliferation and m-hepatocyte death.

To test this possibility we performed the TUNEL analysis and determined the ratios (%) of the $TUNEL^+$ (dead) m-hepatocytes during the repopulation of h-hepatocytes as follows: 0.5 ± 0.1, 0.6 ± 0.2, 1.2 ± 0.1, 0.6 ± 0.3, 0.2 ± 0.1, 3.9 ± 4.7, and 8.5 ± 6.8 at 1, 2, 3, 5, 7, 9, and 11 weeks (each n = 3), respectively. The ratios were quite low until 7 weeks after transplantation and were much lower than those of the $BrdU^+$ h-hepatocytes shown in Figure 1B (~10% at 1 week and ~2% at 7 weeks). Similar TUNEL analysis showed a $TUNEL^+$ ratio of 18.8 ± 6.1% (n = 3) for r-hep-mice at 3 weeks after transplantation, which is con-

siderably higher than that of h-hep-mice at 3 weeks (1.2 ± 0.1%). Based on these analyses, we concluded that the proliferation rate of h-hepatocytes is higher than the death rate of m-hepatocytes, which resulted in the enlargement of liver in h-hep-mice.

Histological Architecture of Sinusoids and Bile Canaliculi in Chimeric Mouse

Liver sinusoids were histologically examined, because their structures reflect the proliferation status of hepatocytes: their structures are compressed[25] and become vague[26] during vigorous hepatocyte proliferation. r-hep- and h-hep$_{9MM}$ Mice were generated and sacrificed in the proliferation (at 2 and 5 weeks after transplantation for r-hep- and h-hep$_{9MM}$ mice, respectively) and proliferation termination phases (at 5 and 14 weeks for r-hep- and h-hep$_{9MM}$ mice, respectively) for histological analysis (Figure 4). Normal livers from Fischer 344 rats and the 65YF donor were used as normal r- and h-liver controls, respectively. H&E sections clearly showed the single-cell structures of hepatic plates in normal r-livers (Figure 4A) and h-livers (Figure 4J). Sections were stained for type IV collagen, an indicator of the subsinusoidal space,[26] and multidrug resistance-associated protein 2 (MRP2), a maker of the canalicular organic anion transporters.[27] These proteins were localized as expected in normal r-livers (Figure 4, B and C) and h-livers (Figure 4, K and L).

H&E-stained sections from r-hep- and h-hep-mouse livers at 5 and 14 weeks, respectively, showed complete repopulation (Figure 4, G and M, respectively), but their histological features were quite different. h-Hepatocytes were less eosinophilic than r-hepatocytes, as reported previously,[7] and swollen and contained less cytoplasm, with wisps of accumulated glycogen, as described previously.[8] Single-cell plates were rarely observable in the

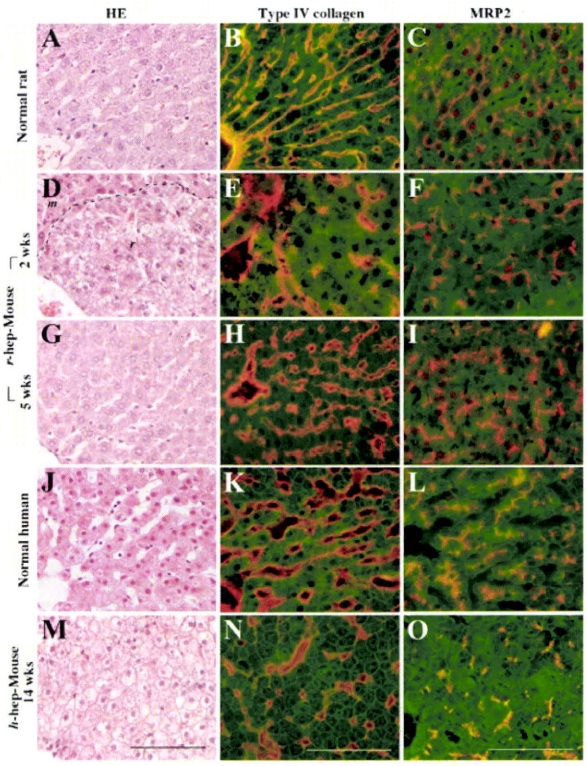

Figure 4. Histological characteristics of r-hep- and h-hep-mouse livers. Normal r- and h-livers were obtained from 13-week-old male Fischer 344 rats (**A–C**) and from a 65YF donor (**J–L**), respectively. r-hep-Mice and h-hep-mice were produced as shown in Figure 1. The former were sacrificed at two (proliferation phase, **D–F**) and five weeks (wks) after transplantation (termination phase, **G–I**) and the latter at 14 weeks (termination phase, **M–O**). Liver sections were stained with H&E (**A**, **D**, **G**, **J**, and **M**) and for type IV collagen (red, **B**, **E**, **H**, **K**, and **N**) and MRP2 (red, **C**, **F**, **I**, **L**, and **O**). The sections from rats and r-hep-mice were additionally stained for rRT1A (green, **B**, **C**, **E**, **F**, **H**, and **I**) and those from the human and h-hep-mice for hCK8/18 (green, **K**, **L**, **N**, and **O**) to identify transplanted r- and h-hepatocytes, respectively. The dashed line in **D** shows the boundary between r-hepatocyte (*r*) and m-hepatocyte regions (*m*). Scale bar = 100 μm.

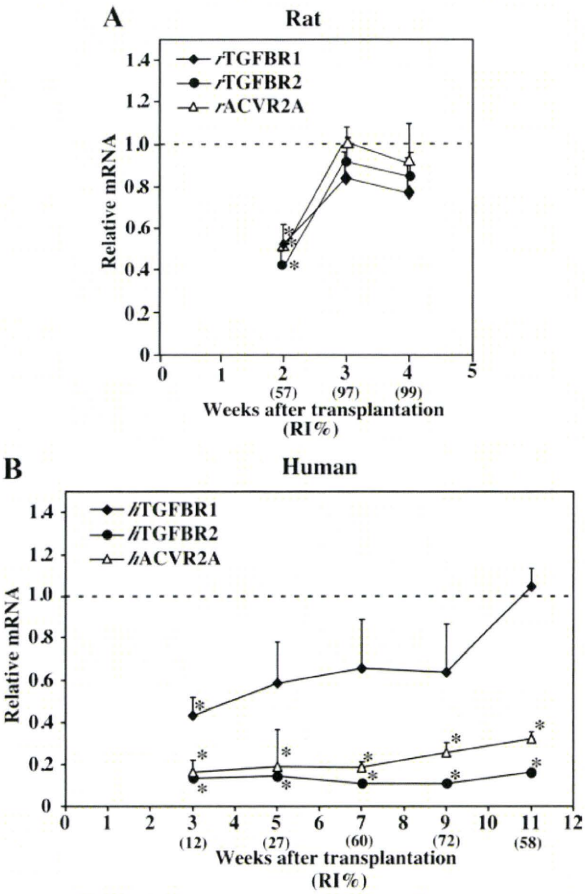

Figure 5. Gene expressions of TGFBR1, TGFBR2, and ACVR2A in r-hep- and h-hep-mouse livers. Real-time RT-PCR was performed by using total mRNA isolated from the livers of r-hep- and h-hep$_{9MM}$ mice shown in Figure 1 as templates, and each result was normalized to that of rGAPDH and hGAPDH. Likewise real-time RT-PCR was performed for liver tissues from 13-week-old male rats and those from the 25YF, 28YM, and 61YF human donors as the normal rat and human controls, respectively. mRNA abundance in r- and h-chimeric mice was divided by that of the normal r- and h-livers, respectively, and is shown as relative mRNA abundance (ordinary axis) in **A** for r-hep-mice and in **B** for h-hep-mice. Normal livers in **A** were obtained from three 13-week-old male rats and those in **B** from three donors, 25YF, 28YM, and 61YF. The dotted horizontal lines show the average expression level in normal livers (1.0). The variations of the normalized rTGFBR1, rTGFBR2, rACVR2, hTGFBR1, hTGFBR2, and hACVR2 were 1.0 ± 0.2, 1.0 ± 0.2, 1.0 ± 0.2, 1.0 ± 0.2, 1.0 ± 0.4, and 1.0 ± 0.2, respectively. Values represent the mean ± SD (n = 3). Significant differences compared with normal livers (*$P < 0.05$). "RI%" shows the average RI calculated from three mice. Closed diamond, TGFBR1; closed circle, TGFBR2; and open triangle, ACVR2A.

h-hepatocyte-regions in h-hep-mice at 14 weeks (Figure 4M), and sinusoids were obscure. Type IV collagen immunostains demonstrated multicell-layer-thick hepatic plates (Figure 4N). The MRP2 protein was randomly distributed in the intercellular space (Figure 4O). Similar histological structures were observed in the h-hepatocyte regions at 5 weeks (data not shown). Likewise sinusoidal structures were not distributed in an orderly fashion in the r-hepatocyte regions of r-hep-mice at 2 weeks when r-hepatocytes were in the proliferation phase (Figure 4, D–F), losing vessel continuity along the portal-central axis. However, r-hep-mice at 5 weeks after transplantation regained the normal arrangement of hepatic plates and sinusoids (Figure 4G), which was consistent with the distributions of type IV collagen and MRP2 (Figure 4, H and I). These proteins were located as in normal r-liver, indicating the reconstruction of the resting liver structure with single hepatic plates along the portal-central axis. These results demonstrate that the h-hepatocytes were incapable of reconstructing the resting liver structure even at 14 weeks after transplantation.

The length of the long axis of hepatocytes was determined on H&E-stained sections from r- and h-hep-mice shown in Figure 4 as a measure of size, which showed no significant differences among m (host)-, r-, and h-hepatocytes in chimeric livers: uPA-expressing m-hepatocytes in h-hep$_{9MM}$ mice at 11 weeks after transplantation, 19.5 ± 4.5 μm (n = 3); uPA-expressing m-hepatocytes in r-hep-mice at 2 weeks, 19.7 ± 4.3 μm (n = 3); r-hepatocytes in r-mice at 5 weeks, 22.7 ± 2.9 μm (n = 3); and h-hepatocytes in h-hep-mice at 11 to 14 weeks, 22.5 ± 1.8 μm (n = 6). This result clearly indicated that the observed enlargement of the h-hep-mouse liver was caused by hyperplasia but not hypertrophy of h-hepatocytes.

TGF-β Signaling in r-hep- and h-hep-Mouse Livers

TGF-β and activin play active roles in the termination of liver regeneration.[14,15,18–20,28] The mRNA expressions of TGFBR1, TGFBR2, and ACVR2A were determined in r-hep-mouse livers at 2, 3, and 4 weeks after transplantation and in h-hep$_{9MM}$ mouse livers at 3, 5, 7, 9, and 11 weeks and compared with those of normal r- and h-liver controls, respectively. In r-hep-mice at 2 weeks (proliferation phase, RI$_{r\text{-}hep}$ = 57%), rTGFBR1, rTGFBR2, and rACVR2A expressions were suppressed to half those of normal r-livers and gradually returned to normal levels at 3 and 4 weeks (termination phase, RI$_{r\text{-}hep}$ = 97 and 99%,

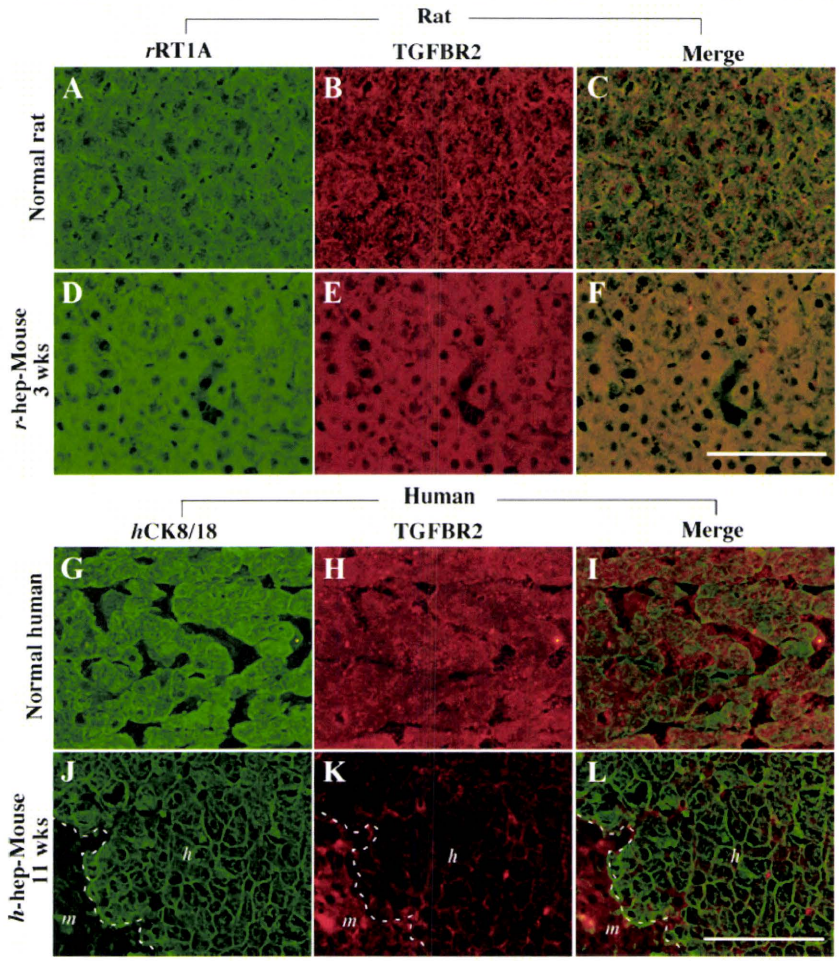

Figure 6. Identification and distribution of TGFBR2 in normal and chimeric livers. uPA/SCID mice were transplanted with r- and h-hepatocytes$_{9MM}$ and sacrificed at 3 and 11 weeks after transplantation, respectively, when the transplanted hepatocytes had terminated proliferation. Two series of double immunohistochemical examinations were performed on liver tissues, one for rat series (Rat) shown in **A–F** that contained normal r-liver (Normal rat) shown in **A–C** and r-hep-mouse liver (**D–F**) and the other for the human series (Human) shown in **G–L** that contained 9MM donor liver as control normal h-liver (Normal human, **G–I**) and h-hep-mouse liver (**J–L**). Liver sections of rat series were double-stained for rRT1A for identifying r-hepatocytes (green; **A** and **D**) and TGFBR2 (red; **B** and **E**) and those of human series for hCK8/18 for identifying h-hepatocytes (green; **G** and **J**) and TGFBR2 (red; **H** and **K**). Images **A** and **B**, **D** and **E**, **G** and **H**, and **J** and **K** were merged and are shown in **C**, **F**, **I**, and **L**, respectively. Similar staining results were obtained from three different mice of each series. The **dashed lines** in **J–L** indicate the boundary between h-hepatocyte (*h*) and m-hepatocyte regions (*m*). Scale bar = 100 μm.

respectively) (Figure 5A) as reported in the regeneration of partial hepatectomized r-liver.[29] In contrast, their expression profiles in h-hep-mouse livers were quite different (Figure 5B). At 3 weeks (proliferation phase, $RI_{h\text{-}hep}$ = 12%), hTGFBR2 and hACVR2A were expressed at levels less than one-third of normal levels; expression remained low throughout the 11-week-long observation period. The suppression of the expression of these genes was reproducible, because similar results were obtained from h-hep-mice generated with another donor (10YF): the ratios of expression levels of hTGFBR2 and hACVR2A in the h-hep-mice at 9 to 11 weeks after transplantation to those in the normal human livers were 0.19 ± 0.05 (n = 3) and 0.19 ± 0.02 (n = 3), respectively. The expression of hTGFBR1 mRNA was high compared with that of these two mRNAs at 3 weeks and gradually increased until reaching the normal levels at 11 weeks.

The expression of TGF-β receptor, TGFBR2, was immunohistochemically examined in r- and h-hep_{9MM} mouse livers at 3 and 11 weeks when the mice showed RI = 97 ± 3% (n = 3) and 58 ± 46% (n = 3), respectively, together with staining for rRT1A and hCK8/18 to identify r- and h-hepatocytes, respectively (Figure 6). As with normal r-hepatocytes (Figure 6, A–C), the $rRT1A^+$ r-hepatocytes in r-hep-mice were stained heavily for TGFBR2 (Figure 6, D–F). Likewise normal h-hepatocytes abundantly expressed TGFBR2 (Figure 6, G–I). In contrast, TGFBR2 was hardly detectable in $hCK8/18^+$ h-hepatocytes in h-hep-mice (Figure 6, J–L). The anti-TGFBR2 antibody used was cross-reactive with r- and m-TGFBR2. The $TGFBR2^+$ cells in the m-hepatocyte region seen in Figure 6K were largely m-hepatocytes according to their morphology. Moderately $TGFBR2^+$ cells in the h-hepatocyte region shown in Figure 6K were mostly m-nonparenchymal cells and few h-hepatocytes (Figure 6, K and L). These results indicated that h-hepatocytes in h-hep-mice maintain low sensitivity to TGF-β, although the expression of TGFBR1 was up-regulated at 11 weeks after transplantation. It is known that TGF-β initially binds to TGFBR2, and TGF-β signals are transferred through the heterodimers of TGFBR1 and TGFBR2.[16] TGF-β-expressing cells were identified in liver sections from r- and h-hep-mice during the proliferation and termination phases by double-immunostaining for desmin and TGF-β (Figure 7). Compared with the control (Figure 7, A–C; normal liver from wild-type SCID mice), tissues collected from the injured livers of uPA/SCID mice contained abundant $desmin^+$ HSCs that were all heavily expressing TGF-β (Figure 7, D–F) as reported previously.[2] Very few $desmin^+$ cells were observed in r-hep-mice at 2 weeks (Figure 7, G–I) or in h-hep-mice at 5 weeks (Figure 7, M–O), suggesting that very few m-HSCs invaded the xenogeneic hepatocyte colonies during the proliferation phase. These cells were all TGF-β^-. m-HSCs increased in number in xenogeneic hepatocyte colonies from both r- and h-hep-mice, particularly in the former, at 3 and 11 weeks (termination phase), respectively (Figure 7, J and P). During the termination phase, m-HSCs in r-hepatocyte colonies from r-hep-mice were TGF-β^+ (Figure 7, J–L). However, importantly, m-HSCs in h-hepatocyte colonies of h-hep-mice were TGF-β^- (Figure 7, P–R). HSCs that express TGF-β should be all m-HSCs in the chimeric mice, because the purity of the transplanted r- or h-hepatocytes was >99%. In r- and h-normal livers, $TGF\text{-}\beta^+$-HSCs were rarely observed (data not shown).

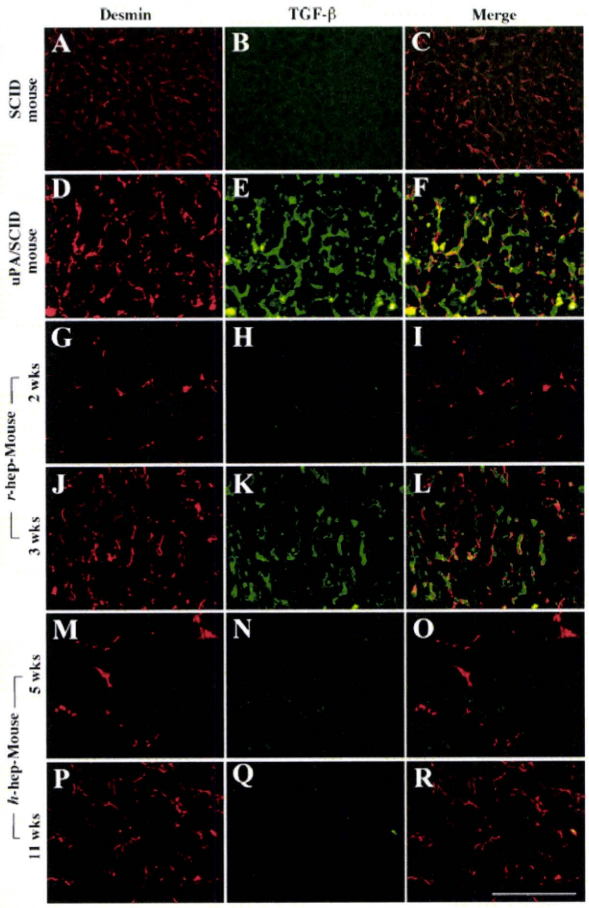

Figure 7. Expression and distribution of TGF-β in normal and chimeric mouse livers. Livers were removed, respectively, from 3-month-old wild-type SCID mice (**A–C**), 1-month-old uPA/SCID mice (**D–F**, injured region), r-hep-mice at 2 (**G–I**) and three (**J–L**) weeks after transplantation, and h-hep-mice at 5 (**M–O**) and 11 weeks (**P–R**). These livers were cryosectioned and double-immunostained for desmin (**A**, **D**, **G**, **J**, **M**, and **P**, red) and TGF-β (**B**, **E**, **H**, **K**, **N**, and **Q**, green). The two sets of photographs are merged and shown in the corresponding panels (**C**, **F**, **I**, **L**, **O**, and **R**) in the **right column**. Serial sections from r- and h-hep-mouse livers were immunostained for rRT1A and hCK8/18 to identify r- and h-hepatocytes, respectively (data not shown). Similar results were obtained from three different mice. Scale bar = 100 μm.

Smad proteins are major intracellular effectors in both TGFBR and ACVR signaling. The distributions of Smad2/3 were examined on liver sections prepared from r- and h-hep-mice at 3 and at 11 weeks (termination phase of r- and h-hep-mice, respectively), respectively, together with liver tissues from Fischer 344 rats and the 49YM donor as normal controls (Figure 8). The nuclei of normal r-livers (Figure 8, A and B) and h-livers (Figure 8, G and H) were both $Smad2^-/3^-$. In contrast, the nuclei of r-hepatocytes in r-hep-mouse were strongly $Smad2^+/3^+$ (Figure 8, D and E), supporting the evidence that r-hepatocytes are activated by TGF-β from m-HSCs. However, as expected, h-hepatocytes showed little or no Smad2/3 immunoreactivity (Figure 8, J and K), suggesting that

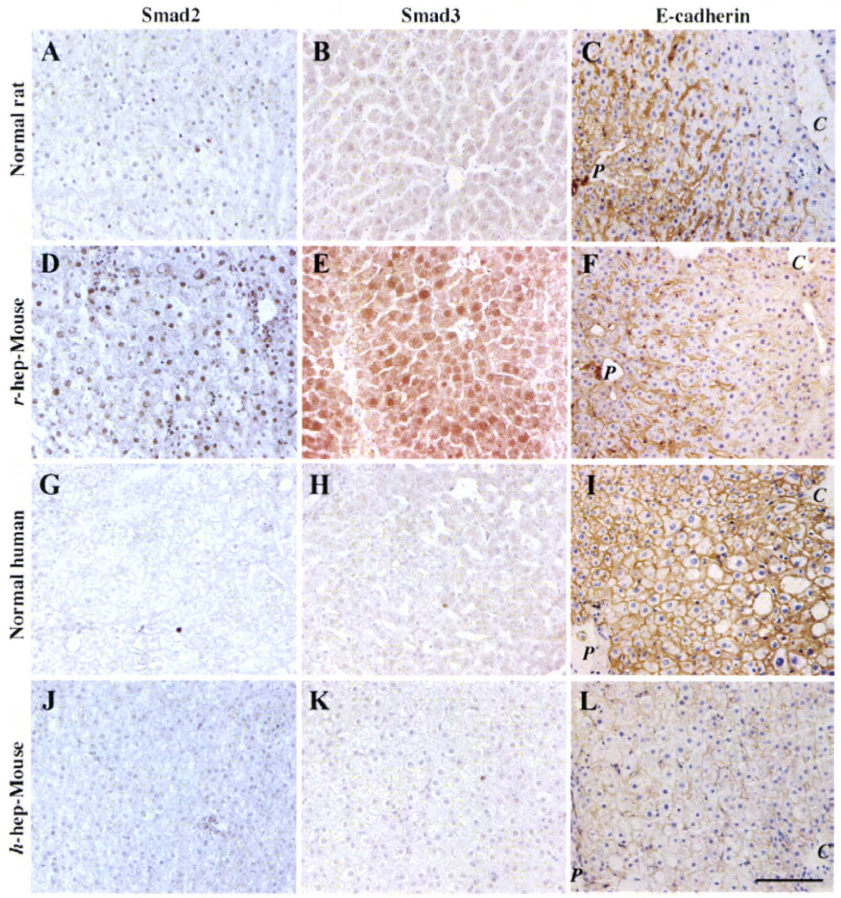

Figure 8. Localization of Smad2/3 and E-cadherin in chimeric mouse liver. Livers were obtained from 13-week-old male Fischer 344 rats (**A–C**, Normal rat), normal donors (49YM, 50YM, and 65YF) (**G–I**, Normal human), r-hep-mice at three weeks (**D** and **E**) and five weeks (**F**), and 9MM-h-hep-mice at 11 weeks (**J** and **K**) and 14 weeks (**L**) after transplantation. They were immunostained for Smad2 (**A**, **D**, **G**, and **J**), Smad3 (**B**, **E**, **H**, and **K**), and E-cadherin (**C**, **F**, **I**, and **L**). Positive signals are brown. Histological examinations were individually performed for these livers in each category, and we obtained similar results. Representative photos are shown here. The photos of Normal human were from 49YM liver. In **C**, **F**, **I**, and **L**, *P* and *C* indicate portal and central veins, respectively. Scale bar = 100 μm.

TGF-β and activin signaling was lacking in h-hep-mice. In h-hep mice from another donor (10YF, 9 to 11 weeks after transplantation), the immunohistological results for TGF-β, Smad2, and Smad3 showed the same tendencies as the results shown in Figures 7 and 8 (data not shown), suggesting that the deficiency of TGF-β signaling is not attributed to the possible immaturity because of the young age (9MM) of the donor.

To obtain an additional evidence for the TGF-β signaling deficiency in h-hep-mice, we examined the expression of E-cadherin in the chimeric mouse, which is one of the TGF-β target genes.[30] Normal r-livers expressed the E-cadherin protein in the periportal zone restrictedly (Figure 8C), and a similar distribution pattern was observed in the r-hep-mouse livers (Figure 8F). In contrast to normal r-livers, normal h-livers uniformly and evenly expressed E-cadherin (Figure 8I). Its expression was significantly low in the h-hepatocyte region of the h-hep-mouse liver (Figure 8I) compared with that in the normal h-livers.

Participation of m-HSCs in the Donor Hepatocyte Colonies

As shown in Figure 7, the xenogeneic hepatocyte regions contained fewer m-HSCs than the injured host regions, especially in the proliferation phase. We further investigated this phenomenon using desmin as a HSC marker. The desmin$^+$ cells were scarce in both r- and h-hepatocyte colonies in r-hep-mice at 2 weeks (Figure 9A) and in h-hep-mice at 5 weeks after transplantation (Figure 9B), respectively, compared with the degenerating m-hepatocyte regions that surrounded the corresponding donor cell regions. These xenogeneic hepatocytes were both in the proliferation phase (Figure 1). This paucity of HSCs seemed to be related to the fact that the sinusoids were still under reconstruction (Figure 4E) in r-hep-mouse liver at 2 weeks and in h-hep-mouse liver at 5 weeks (data not shown). HSCs were abundant in r-hepatocyte colonies in r-hep-mice at 3 weeks (termination phase) (Figure 9C), supporting the result of Figure 7J. The HSCs also increased in density in h-hepatocyte colonies of h-hep-mice at 11 weeks (Figure 9D), also supporting the result of Figure 7P. However, the density was apparently lower than that in r-hepatocyte colonies, most probably reflecting the fact that the sinusoids were less developed than in r-hepatocyte colonies in the termination phase (Figure 4N versus Figure 4H, respectively). These desmin$^+$ HSCs were not derived from h-HSCs, because, first the purity of the transplanted h-hepatocytes was >99% and second h-HSCs do not express desmin.[31] The m-HSC-occupied areas (red-colored areas) were measured in the entire normal mouse (wild-type SCID mouse) liver (control) and in the xenogeneic hepatocyte regions of chimeric livers on immunostained sections. The ratios (R_{HSC}) of red-colored areas

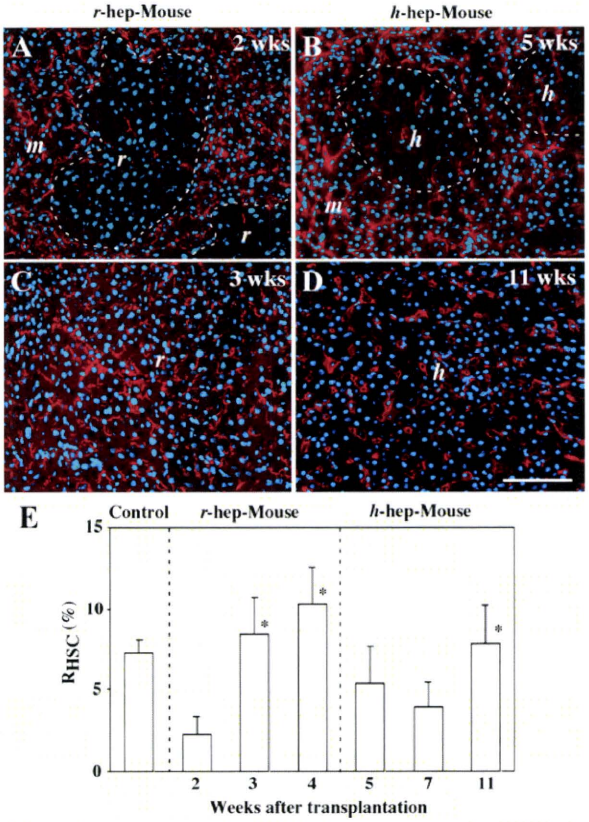

Figure 9. Distribution of m-HSCs in r- and h-hep-mice. Liver sections from r-hep-mice at two (proliferation phase, **A**) and three (termination phase, **C**) weeks and from 9MM h-hep-mice at five (proliferation phase, **B**) and 11 (termination phase, **D**) weeks after transplantation were immunostained for desmin (red). The nuclei were stained with Hoechst 33258 (blue). Serial sections from the r-hep- and h-hep-mouse livers were immunostained for rRT1A and hCK8/18 to identify r-and h-hepatocytes, respectively (data not shown), from which the boundary between the host (*m*) and transplanted (*r* or *h*) hepatocyte regions was determined, as indicated by the **dashed lines** in **A** and **B**. Similar results were obtained from three different mice. Scale bar = 100 μm. **E:** Changes in the ratio of desmin$^+$ cells in xenogeneic hepatocyte regions during liver repopulation. Liver sections from 3-month-old wild-type SCID mice (control), r-, and h-hep-mice at the indicated weeks after transplantation were immunostained for desmin. Serial sections were stained with anti-rRT1A and -hCK8/18 antibodies to identify r- and h-hepatocytes, respectively. The ratio (R_{HSC}) of desmin$^+$ areas over the measured areas was calculated in the xenogeneic hepatocyte region using NIH imaging software and is expressed as a percentage. Data represent the mean ± SD of desmin$^+$ area per section in a total of 15 randomly selected fields ($n = 3$). **Asterisks** at three and four weeks in the panel for r-hep-mice indicate significant differences versus the value at two weeks. The **asterisk** at 11 weeks in the panel of h-hep-mice indicates a significant difference versus the value at five weeks.

to either the entire liver of SCID mouse or to the xenogeneic region of chimeric liver were calculated and are shown in Figure 9E. The R_{HSC} in normal mice was 7.3 ± 0.8%. In r-hep-mice, the R_{HSC} was 2.3 ± 1.1% at 2 weeks and increased to 10.3 ± 2.3% at 4 weeks. In h-hep-mice, the R_{HSC} was approximately 5% for up to 7 weeks and significantly increased to 7.8 ± 2.4% ($P < 0.01$) at 11 weeks. The R_{HSC} of r-hep-mice at 4 weeks was significantly higher than that of h-hep-mice at 11 weeks ($P < 0.01$).

Discussion

In this study, we compared the repopulation processes between r- and h-hepatocytes in the livers of uPA/SCID mice and showed several physiologically significant differences. The r-hepatocytes rapidly replaced m-hepatocytes to keep a normal $R_{L/B}$, suggesting a repopulation in a strictly regulated manner. The r-hepatocytes expressed TGFBR1/2 mRNAs at lower levels in the proliferation phase and then gradually increased expressions in the termination phase when m-HSCs actively expressed TGF-β. Moreover, Smad2/3 were translocated in r-hepatocyte nuclei, suggesting that TGF-β/TGFBR/Smad signaling normally works as in the terminal phase of mouse liver regeneration.

In the chimeric animal h-hepatocytes were quite different from r-hepatocytes. They proliferated much slowly, requiring approximately four times longer to complete proliferation than r-hepatocytes. The resulting liver showed marked overgrowth compared with a normal m-liver. TGFBR2 and ACVR2A, and TGF-β were not up-regulated in h-hepatocytes and m-HSCs of h-hep-mice, respectively, in the termination phase, indicating the absence of physiologically meaningful signaling between h-hepatocytes and m-HSCs. The density of m-HSCs in h-hepatocyte colonies was lower than that in r-hepatocyte colonies even in the termination phase, which probably reflects the poor development of sinusoids in h-hep-mice, because the multiple hepatic plates would result in the lower volume of the space of Disse than in the liver with single hepatic plates. It has been reported that intimate signaling between hepatocytes and nonparenchymal cells plays an important role in the termination of liver regeneration.[32] Thus, the failure of m-HSCs to express TGF-β could be a cause of liver hyperplasia of h-hep-mice. However, it is appropriate to note here that other factors such as hepatocyte growth factor[33] and bile acids[34] might be involved in the observed hyperplasia.

In TGFBR2 knockout mice, partial hepatectomy resulted in a 1.2-fold increase beyond the normal liver weight because of a compensatory increase in activin A/ACVR2A signaling and persistent activity in the Smad pathway.[20] Unlike in the study cited, the levels of ACVR2A mRNA and Smad proteins remained low through the experimental period in the present study with h-hep-mice. Thus, the lack of both TGF-β and activin signaling may have been partly responsible for the observed overgrowth of hepatocytes. We did not observe any symptoms of carcinogenic transformation in h-hepatocytes (data not shown), although TGFBR2[35] and ACVR2[36] are putative tumor suppressors, suggesting a requirement for additional factor(s) for hepatocarcinogenesis.

Even in the absence of TGF-β/TGFBR signaling, the transplanted h-hepatocytes eventually terminated proliferation. The histological features of sinusoids and canaliculi in mouse liver repopulated by xenogeneic hepatocytes demonstrated that h-hepatocytes did not restore the normal arrangement of single hepatic plates in the resting phase of the liver, but they formed multiple hepatic plates seen in the regenerating liver.[25,26] Thus, it is most likely that h-hepatocytes eventually terminated the proliferation because of contact inhibition within the multiple hepatocyte layers. r-Hepatocytes also formed multiple hepatic plates in the proliferation phase but restored the normal structures of single cell plates along the portal-central axis in the termination phase. It seems that

TGF-β/TGFBR signaling is required for both the formation of single hepatic plates and the normal termination of liver growth. These apparently distinct events (liver growth termination and hepatic plate structuring) should be closely related at the molecular levels, because adhesion molecules such as E-cadherin and β1-integrin are reported as the Smad2/3-mediated TGF-β target genes in liver development.[30] Our results demonstrated that E-cadherin uniformly exists on the hepatocyte surfaces in the normal h-liver, but its expression was quite low in substantial portions of the h-hepatocyte region in the h-hep-mouse liver. It is likely that this expression defect in the cell adhesion molecule results in abnormal hepatocyte plate arrangements. Loss of TGF-β signaling in h-hep-mice might be responsible for the maintenance of multicell-thick hepatic plates after the termination of liver repopulation in the h-hep-mouse livers.

There is the possibility that the observed hyperplasia of h-hepatocytes is the result of a signaling failure between m-cytokine ligands and the corresponding h-receptors. Recently, we showed that h-hepatocytes in h-hep-mice are growth hormone-deficient, because mouse growth hormone does not recognize the human growth hormone receptor of h-hepatocytes.[37] However, we consider that h-hepatocytes would be able to respond to TGF-β if the host m-HSCs secreted it, because there has been no report of species specificity between h- and m-TGF-β. In the present study we clearly demonstrated the coincidence of lack of TGF-β/TGFBR signaling with the hyperplasia of h-hep-mouse liver. However, the direct causality between such signaling and the liver hyperplasia remains to be examined. It is well known that hepatocytes and stellate cells interact with each other through varieties of signaling molecules and together contribute to physiological and pathological changes of liver. Therefore, we conclude that the lack of or weak interaction between h-hepatocytes and m-HSCs, which we have revealed at the histological and gene/protein expression levels, is responsible for the presently observed hyperplasia of h-hep-mouse liver.

Xenotransplantation, such as from pigs to humans, could potentially compensate for the lack of human organ and tissue donors. Our results indicate that, in addition to potential immunological rejection, the transplanted cells or tissues may fail to interact appropriately with the host environment. We propose that the h-chimeric mouse is a useful model for not only examining the mechanism of liver regeneration but also studying risks of xenotransplantation.

Acknowledgments

We thank Yasumi Yoshizane, Hiromi Kohno, Yoko Matsumoto, and Sanae Nagai for technical assistance and Dr. Masumi Yamada for helpful discussion and comments.

References

1. Heckel JL, Sandgren EP, Degen JL, Palmiter RD, Brinster RL: Neonatal bleeding in transgenic mice expressing urokinase-type plasminogen activator. Cell 1990, 62:447–456
2. Locaputo S, Carrick TL, Bezerra JA: Zonal regulation of gene expression during liver regeneration of urokinase transgenic mice. Hepatology 1999, 29:1106–1113
3. Rhim JA, Sandgren EP, Degen JL, Palmiter RD, Brinster RL: Replacement of diseased mouse liver by hepatic cell transplantation. Science 1994, 263:1149–1152
4. Rhim JA, Sandgren EP, Palmiter RD, Brinster RL: Complete reconstitution of mouse liver with xenogeneic hepatocytes. Proc Natl Acad Sci USA 1995, 92:4942–4946
5. Dandri M, Burda MR, Gocht A, Török E, Pollok JM, Rogler CE, Will H, Petersen J: Woodchuck hepatocytes remain permissive for hepadnavirus infection and mouse liver repopulation after cryopreservation. Hepatology 2001, 34:824–833
6. Dandri M, Burda MR, Török E, Pollok JM, Iwanska A, Sommer G, Rogiers X, Rogler CE, Gupta S, Will H, Greten H, Petersen J: Repopulation of mouse liver with human hepatocytes and in vivo infection with hepatitis B virus. Hepatology 2001, 33:981–988
7. Tateno C, Yoshizane Y, Saito N, Kataoka M, Utoh R, Yamasaki C, Tachibana A, Soeno Y, Asahina K, Hino H, Asahara T, Yokoi T, Furukawa I, Yoshizato K: Near completely humanized liver in mice shows human-type metabolic responses to drugs. Am J Pathol 2004, 165:901–912
8. Meuleman P, Libbrecht L, De Vos R, de Hemptinne B, Gevaert K, Vandekerckhove J, Roskams T, Leroux-Roels G: Morphological and biochemical characterization of a human liver in an uPA-SCID mouse chimera. Hepatology 2005, 41:847–856
9. Emoto K, Tateno C, Hino H, Amano H, Imaoka Y, Asahina K, Asahara T, Yoshizato K: Efficient in vivo xenogeneic retroviral vector-mediated gene transduction into human hepatocytes. Hum Gene Ther 2005, 16:1168–1674
10. Kam I, Lynch S, Svanas G, Todo S, Polimeno L, Francavilla A, Penkrot RJ, Takaya S, Ericzon BG, Starzl TE, Van Thiel DH: Evidence that host size determines liver size: studies in dogs receiving orthotopic liver transplants. Hepatology 1987, 7:362–366
11. Van Thiel DH, Gavaler JS, Kam I, Francavilla A, Polimeno L, Schade RR, Smith J, Diven W, Penkrot RJ, Starzl TE: Rapid growth of an intact human liver transplanted into a recipient larger than the donor. Gastroenterology 1987, 93:1414–1419
12. Francavilla A, Zeng Q, Polimeno L, Carr BI, Sun D, Porter KA, Van Thiel DH, Starzl TE: Small-for-size liver transplantation into large recipient: a model of hepatic regeneration. Hepatology 1994, 19:210–216
13. Nakamura I, Tomita Y, Hirai R, Yamaoka K, Kaji K, Ichihara A: Inhibitory effect of transforming growth factor-β on DNA synthesis of adult rat hepatocytes in primary culture. Biochem Biophys Res Commun 1985, 133:1042–1050
14. Russell WE, Coffey RJ Jr., Ouellette AJ, Moses HL: Type β transforming growth factor reversibly inhibits the early proliferative response to partial hepatectomy in the rat. Proc Natl Acad Sci USA 1988, 85:5126–5130
15. Zhang YQ, Kanzaki M, Mashima H, Mine T, Kojima I: Norepinephrine reverses the effects of activin A on DNA synthesis and apoptosis in cultured rat hepatocytes. Hepatology 1996, 23:288–293
16. Hu PP, Datto MB, Wang XF: Molecular mechanisms of transforming growth factor-β signaling. Endocr Rev 1998, 19:349–363
17. Kumar A, Novoselov V, Celeste AJ, Wolfman NM, ten Dijke P, Kuehn MR: Nodal signaling uses activin and transforming growth factor-β receptor-regulated Smads. J Biol Chem 2001, 276:656–661
18. Braun L, Mead JE, Panzica M, Mikumo R, Bell GI, Fausto N: Transforming growth factor β mRNA increases during liver regeneration: a possible paracrine mechanism of growth regulation. Proc Natl Acad Sci USA 1988, 85:1539–1543
19. Romero-Gallo J, Sozmen EG, Chytil A, Russell WE, Whitehead R, Parks WT, Holdren MS, Her MF, Gautam S, Magnuson M, Moses HL, Grady WM: Inactivation of TGF-β signaling in hepatocytes results in an increased proliferative response after partial hepatectomy. Oncogene 2005, 24:3028–3041
20. Oe S, Lemmer ER, Conner EA, Factor VM, Levéen P, Larsson J, Karlsson S, Thorgeirsson SS: Intact signaling by transforming growth factor β is not required for termination of liver regeneration in mice. Hepatology 2004, 40:1098–1105
21. Hino H, Tateno C, Sato H, Yamasaki C, Katayama S, Kohashi T, Aratani A, Asahara T, Dohi K, Yoshizato K: A long-term culture of human hepatocytes which show a high growth potential and express

their differentiated phenotypes. Biochem Biophys Res Commun 1999, 256:184–191
22. Seglen PO: Preparation of isolated rat liver cells. Methods Cell Biol 1976, 13:29–83
23. Utoh R, Tateno C, Yamasaki C, Hiraga N, Kataoka M, Shimada T, Chayama K, Yoshizato K: Susceptibility of chimeric mice with livers repopulated by serially subcultured human hepatocytes to hepatitis B virus. Hepatology 2008, 47:435–446
24. Livak KJ, Schmittgen TD: Analysis of relative gene expression data using real-time quantitative PCR and the $2^{-\Delta\Delta C}$ method. Methods 2001, 25:402–408
25. Wack KE, Ross MA, Zegarra V, Sysko LR, Watkins SC, Stolz DB: Sinusoidal ultrastructure evaluated during the revascularization of regenerating rat liver. Hepatology 2001, 33:363–378
26. Martinez-Hernandez A, Delgado FM, Amenta PS: The extracellular matrix in hepatic regeneration. Localization of collagen types I, III, IV, laminin, and fibronectin. Lab Invest 1991, 64:157–166
27. Keppler D, Konig J: Hepatic canalicular membrane 5: expression and localization of the conjugate export pump encoded by the MRP2 (cMRP/cMOAT) gene in liver. FASEB J 1997, 11:509–516
28. Michalopoulos GK: Liver regeneration. J Cell Physiol 2007, 213: 286–300
29. Chari RS, Price DT, Sue SR, Meyers WC, Jirtle RL: Down-regulation of transforming growth factor beta receptor type I, II, and III during liver regeneration. Am J Surg 1995, 169:126–132
30. Weinstein M, Monga SP, Liu Y, Brodie SG, Tang Y, Li C, Mishra L, Deng CX: Smad proteins and hepatocyte growth factor control parallel regulatory pathways that converge on β1-integrin to promote normal liver development. Mol Cell Biol 2001, 21:5122–5131
31. Cassiman D, Libbrecht L, Desmet V, Denef C, Roskams T: Hepatic stellate cell/myofibroblast subpopulations in fibrotic human and rat livers. J Hepatol 2002, 36:200–209
32. Koniaris LG, McKillop IH, Schwartz SI, Zimmers TA: Liver regeneration. J Am Coll Surg 2003, 197:634–659
33. Patijn GA, Lieber A, Schowalter DB, Schwall R, Kay MA: Hepatocyte growth factor induces hepatocyte proliferation in vivo and allows for efficient retroviral-mediated gene transfer in mice. Hepatology 1998, 28:707–716
34. Huang W, Ma K, Zhang J, Qatanani M, Cuvillier J, Liu J, Dong B, Huang X, Moore DD: Nuclear receptor–dependent bile acid signaling is required for normal liver regeneration. Science 2006, 312:233–236
35. Derynck R, Akhurst RJ, Balmain A: TGF-β signaling in tumor suppression and cancer progression. Nat Genet 2001, 29:117–129
36. Jeruss JS, Sturgis CD, Rademaker AW, Woodruff TK: Down-regulation of activin, activin receptors, and Smads in high-grade breast cancer. Cancer Res 2003, 63:3783–3790
37. Masumoto N, Tateno C, Tachibana A, Utoh R, Morikawa Y, Shimada T, Momisako H, Itamoto T, Asahara T, Yoshizato K: GH enhances proliferation of human hepatocytes grafted into immunodeficient mice with damaged liver. J Endocrinol 2007, 194:529–553

World Journal of Gastroenterology

Online Submissions: http://www.wjgnet.com/1007-9327office
wjg@wjgnet.com
doi:10.3748/wjg.v16.i23.2851

World J Gastroenterol 2010 June 21; 16(23): 2851-2866
ISSN 1007-9327 (print)

Fixation methods for electron microscopy of human and other liver

Eddie Wisse, Filip Braet, Hans Duimel, Celien Vreuls, Ger Koek, Steven WM Olde Damink, Maartje AJ van den Broek, Bart De Geest, Cees HC Dejong, Chise Tateno, Peter Frederik

Eddie Wisse, Hans Duimel, Celien Vreuls, Peter Frederik, Electron Microscope Unit, University of Maastricht, 6200 MD Maastricht, The Netherlands
Eddie Wisse, Filip Braet, Australian Key Center for Microscopy and Microanalysis, Sydney University, NSW 2006 Sydney, Australia
Eddie Wisse, Ger Koek, Department of Internal Medicine, University of Maastricht, 6200 MD Maastricht, The Netherlands
Steven WM Olde Damink, Maartje AJ van den Broek, Cees HC Dejong, Department of Surgery, University of Maastricht, 6200 MD Maastricht, The Netherlands
Bart De Geest, Center for Molecular and Vascular Biology, University of Leuven, 3000 Leuven, Belgium
Chise Tateno, PhoenixBio Co., 3-4-1 Kagamiyama, Higashi-Hiroshima 739-0046, Japan
Author contributions: Wisse E and Braet F designed the fixation procedures and wrote the manuscript together; Wisse E performed the EM observations; Braet F provided the schematic diagrams; Duimel H and Vreuls C prepared the specimens and sections and provided technical support; Olde Damink SWM, Dejong CHC, van den Broek MAJ and Koek G provided the human liver wedge biopsies, obtained approval of the ethical committee and provided the clinical data; De Geest B provided rabbit, mouse and human livers and biopsies; Tateno C provided mouse livers of different strains; Frederik P supervised the study as head of the EM Unit.
Correspondence to: Dr. Eddie Wisse, Professor, Electron Microscope Unit, University of Maastricht, PO Box 616, 6200 MD Maastricht, The Netherlands. eddie@wisse.be
Telephone: +31-43-3881280 Fax: +31-43-3671040
Received: December 29, 2009 Revised: January 25, 2010
Accepted: February 1, 2010
Published online: June 21, 2010

Abstract

For an electron microscopic study of the liver, expertise and complicated, time-consuming processing of hepatic tissues and cells is needed. The interpretation of electron microscopy (EM) images requires knowledge of the liver fine structure and experience with the numerous artifacts in fixation, embedding, sectioning, contrast staining and microscopic imaging. Hence, the aim of this paper is to present a detailed summary of different methods for the preparation of hepatic cells and tissue, for the purpose of preserving long-standing expertise and to encourage new investigators and clinicians to include EM studies of liver cells and tissue in their projects.

Key words: Liver; Tissue fixation; Perfusion; Electron microscopy; Biopsy

Peer reviewer: Dr. Lisardo Boscá, Professor, Instituto de Investigaciones Biomédicas Alberto Sols (CSIC-UAM), Arturo Duperier 4, 28029 Madrid, Spain

Wisse E, Braet F, Duimel H, Vreuls C, Koek G, Olde Damink SWM, van den Broek MAJ, De Geest B, Dejong CHC, Tateno C, Frederik P. Fixation methods for electron microscopy of human and other liver. *World J Gastroenterol* 2010; 16(23): 2851-2866 Available from: URL: http://www.wjgnet.com/1007-9327/full/v16/i23/2851.htm DOI: http://dx.doi.org/10.3748/wjg.v16.i23.2851

INTRODUCTION

For an electron microscopic study of the liver, expertise and complicated, time-consuming processing of hepatic cells and tissues is needed. The interpretation of electron microscopy (EM) images requires knowledge of the liver fine structure and experience with the numerous artifacts in fixation, embedding, sectioning, contrast staining and microscopic imaging. In addition, the considerable investment in equipment and the costs of personnel, together with the construction and maintenance of dedicated laboratory space and accessory equipment, makes EM investigation of cells and tissues one of the most cost-intensive approaches in biomedical research. The choice of the

right preparation method and the use of good criteria to evaluate the quality of the preparation, together with the right interpretation of the results, is crucial not only for getting the best out of the method, but also to avoid misuse of tax payers money. With sadness, we conclude that the old trade of traditional EM studies is disappearing, and is being partly replaced by immunological techniques and confocal or fluorescence microscopy[1,2]. Hence, the aim of this special paper is to present a detailed summary of different methods for the preparation of hepatic cells and tissue, for the sake of preserving long-standing expertise and to encourage new investigators and clinicians to include EM studies of liver cells and tissue in their projects. In a recent review and guidelines on the clinical use of liver needle biopsies by Rockey *et al*[3], it is stated that, at present, there is only a minor or even negligible role for the use of EM in the diagnosis, prognosis and management of patients with liver disease.

METHODS OF FIXATION AND PREPARATION

Fixation has several goals: (1) to stop metabolism; (2) to fix structures of organelles and molecules in their current position; and (3) to make material accessible and stable during further processing. When metabolic activity in tissues is not arrested, autolytic changes will develop within minutes or even seconds. The need to use extremely fresh tissue, preferably without touching and deformation is therefore of utmost importance. The fixation is also responsible for crosslinking and arresting many molecules with the result that cells, organelles and their substructures are preserved. After embedding, sectioning and contrast staining, these structures become visualized in the electron microscope at magnifications in the range of 50 to 1 000 000 times. The protocols given hereafter can be used for light microscopy, scanning electron microscopy (SEM) and transmission electron microscopy (TEM).

In a situation where experimental animals are used, the method of perfusing a fixative through the portal vein is by far the best method to choose[4-7]. When a complete liver is not available, injecting the fixative into a piece of tissue not smaller than 1 cm provides comparable results to portal vein perfusion. This method can be applied to experimental or clinical wedge biopsies[8-13]. An advantage of this method is the fact that it only requires a small opening of the peritoneal wall to collect a small piece of tissue. With regard to needle biopsies, there have been attempts to inject the fixative into the tissue of the biopsy, with quite good results[8,10,12,14-16]. Unfortunately, these attempts have not resulted in routine applications and immersion fixation remained the standard method of fixing liver needle biopsy specimens. Vascular perfusion through a partly resected liver not used for transplantation, has also been reported to be successful[17]. In order to complete the series of protocols, we have added a short description of fixation of liver cell cultures.

Important elements in fixation are the chemical composition of fluids and the physical conditions during their application. Fluids involved in the fixation process should be isotonic to the cells; in other words, the fixation fluid should be as physiological as possible, with the exception of the fixing compound[18]. To avoid temperature shock of cells and tissues before the actual fixation sets in, isothermic fluids should be used in principle. The major condition for fixation is to transfer cells and tissues from their natural environment to the fixing environment, as rapidly as possible: this should take not more than a few seconds, be it in the operating room or in the laboratory. Living cells and tissues should not be left alone, not even for a few seconds, when this can be avoided. One should avoid subjecting the cells or tissue to drying or dry conditions, keep them wet and well-immersed in fluid, and watch the meniscus carefully to ensure that it does not touch the cells, because it will destroy them.

Fixation should be applied at the cellular level, i.e. bring all cells instantaneously and simultaneously into contact with the fixative. Immersion fixation of small pieces of tissue by plunging them into a fixative has to be avoided as much as possible. The slow penetration of a fixative into a 1-mm piece of tissue results in bad fixation in the center of the block. During the penetration of the fixative, its constituents react differently with cellular components, thereby changing the composition of the fixative on its way to the center of the block. The vehicle (buffer) is supposed to penetrate more rapidly, at the same time slowing down the fixing compound. Immersion fixation might leave the center of a tissue block unfixed for the major part of an hour. Nevertheless, immersion-fixed liver biopsies might provide sufficient information on the ultrastructure of parenchymal cells, but unfortunately sinusoids and sinusoidal cells are destroyed by immersion fixation.

Perfusion protocols allow a regimen of different fluids to be flushed through the liver[18]. Since osmium is an expensive and very toxic substance, it is not recommended to apply this fixative by perfusion. We have tried osmium perfusion[4], but the results were poor[18]. For post-fixation, the tissue should be cut into pieces that are washed in buffer to avoid chemical reactions between glutaraldehyde and osmium. The tissue blocks are subsequently immersed in the buffered osmium tetroxide. By doing so, one has control over a toxic procedure, while there is free admission of osmium to the cells through open veins and sinusoids, and the rapid application of a second fixative with a different reaction mechanism[19]. Although ethanol is used to dehydrate the tissue, its capacity to precipitate proteins and harden the tissue contributes to the fixation process. In order to better preserve membranes and their contrast, several additives to the fixatives have been proposed and applied, such as Ca^{2+} or Li^{+} ions, ferrocyanide[20], tannic acid, and picric acid[19,21].

Cryotechniques, molecular identification of cellular components, and their three-dimensional reconstruction or cryofracture as an alternative method to chemical fixation are not the subject of this review.

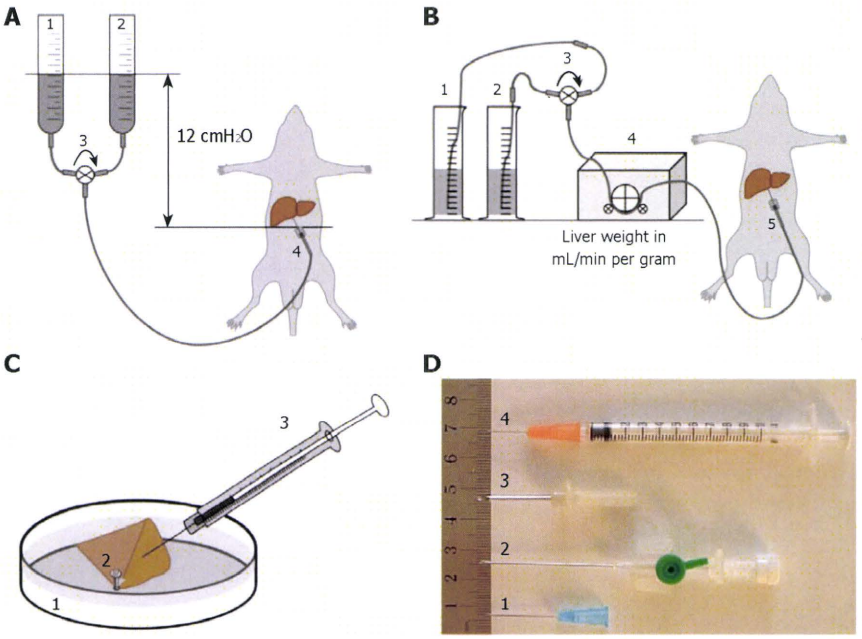

Figure 1 Diagram schematically depicting the different and most frequently used perfusion-fixation methods, including perfusion-fixation needles, to fix hepatic tissue. A: Gravity-mediated perfusion fixation using 12 cm water pressure: (1) pre-perfusion buffer; (2) fixative solution; (3) tri-valve system (e.g. Discofix® C, B. Braun, Switzerland) that facilitates the change-over between both solutions; and (4) cannulation of the portal vein; B: Roller pump-mediated perfusion fixation at a flow of 1 mL/g liver tissue: (1) pre-perfusion buffer; (2) fixative solution; (3) tri-valve system; (4) low-flow peristaltic pump; and (5) cannulation of the portal vein; C: Injection or puncture perfusion fixation, using a needle to inject fixative into a wedge biopsy of about 1 cm × 1 cm × 1 cm dimensions. Injection to approach a rate of 1 mL/min: (1) Petri dish filled with 37℃ physiological saline solution; (2) liver tissue wedge fixed by the tip of a forceps; and (3) syringe containing fixative solution; D: Different types of needles and their variants commonly used for portal vein insertion: (1) 18-23 G needle typically used for gravity-mediated perfusion for rat and mouse livers; (2) 18 G needle catheters are recommended for peristaltic-pump-mediated perfusion; (3) 12-13 G needles are typically used for larger animals such as rabbits; and (4) 25 G syringes are ideal for the injection of fixative solution in hepatic tissue. In case of accidental failure of procedure A or B, method C (injection perfusion) can be used to save the preparation.

FIXATION PROTOCOLS

Perfusion fixation of total liver in situ (mostly applied to experimental animals)[5,6,22,23]

The procedure for perfusion fixation of total liver *in situ* is as follows: (1) Anesthetize the animal, preferably with 4.5 mg/100 g body weight Nembutal (which also relaxes the musculature); (2) Fix the animal to a waterproof surgical support with its back down; (3) Shave and disinfect the animal's abdomen; (4) Open the abdominal cavity along the linea alba, with lateral cuts along the ribs and lower segment; (5) Gently move the intestines aside and cover them with surgical cotton or bandages wetted with warm physiological saline to keep them moist and warm (one could also use an infrared lamp); (6) Expose the portal vein and prepare separate, double ligatures around it; (7) Take care that the hepatic artery is included in the ligature; (8) Introduce the largest possible (just fitting) needle into the portal vein, after connecting it to a silicon tube that is connected to the perfusion system (fluids on room temperature, glass vessels or peristaltic pump, Figure 1A and B); (9) Constrict the ligatures independently, taking care not to puncture the portal vein, and make sure to close to the hepatic artery; (10) Start perfusion with glutaraldehyde solution by opening a valve or switching on the peristaltic pump; the flow rate in mL/min should be more or less equal the total weight of the liver in grams; (11) Incise the vena cava to allow fluids to escape from the vascular system, and aspirate fluids when necessary; (12) Watch the liver change in color and consistency. This process should start within the first minute (typically 15-30 s); (13) Stop the perfusion after 5 min; (14) Gently remove the liver or one or two well-perfused lobes and put them into a Petri dish that contains fixative. Well-perfused liver lobes change their color from dark red to yellow/brown, whereas the consistency changes from soft to hard like a boiled egg. Badly perfused parts of the liver that are entirely or partly soft and still dark red-brown in color should not be processed. Note that some lobes, e.g. the caudate lobe, often show better perfusion than other ones; (15) Clean a razor blade with ethanol and paper tissue (to remove protecting grease) and gently cut 1-mm slices of liver tissue. Do not put any pressure on the tissue while cutting, and make sawing movements with the razor blade; (16) Keep tissue slices covered with glutaraldehyde and cut multiple 1 mm × 1 mm strips under fluid; (17) Cut several strips simultaneously into 1 mm × 1 mm × 1 mm blocks for TEM, or 1 mm × 1 mm × 5 mm strips for SEM and/or 5 mm × 5 mm × 1 mm slices for light microscopy (LM) flat embedding; (18) Total time in glutaraldehyde should not be longer than 20 min; (19) Transfer blocks to washing buffer (which is the buffer of the glutaraldehyde fixative) to remove glutaraldehyde before contact with osmium; (20) Transfer blocks to 1% buffered osmium in small glass vessels and close these with a cap; (21) Postfix for 1 h in osmium, keep the small vessels at 4℃, and shake

Table 1 Dehydration and embedding for TEM and SEM

TEM		
Ethanol 70%	15 min	20℃
Ethanol 90%	15 min	20℃
Ethanol 100%	30 min	20℃
Ethanol 100%	30 min	20℃
Ethanol 100%/Epon 1/1	Overnight	20℃
Epon	1 h	20℃
Epon 1 (overnight)	BEEM capsules on top	20℃
Epon	Fill BEEM capsules	20℃
Oven	67 h	40-60℃
SEM		
Ethanol 70%	15 min	20℃
Ethanol 90%	15 min	20℃
Ethanol 100%	30 min	20℃
Ethanol 100%	30 min	20℃
Ethanol 100%	Overnight	20℃
Freeze and fracture	Liquid nitrogen	-196℃
Ethanol 100%	30 min	20℃
Critical point drying, phase 1	CO_2/ethanol	16℃
Phase 2 or HDMS drying (see below)	80 bar	35℃
Sputter coating	Pt/Au	

Cutting of ultrathin sections on an ultramicrotome, contrast staining with lead and uranyl salts. TEM: Transmission electron microscopy; SEM: Scanning electron microscopy.

the fluid gently and regularly; (22) Transfer the tissue blocks to the second washing buffer (osmium-vehicle buffer), and wash once or twice to remove osmium; (23) Transfer the blocks to 70% ethanol (v/v); (24) Change 70% ethanol three times; and (25) Transport in 70% ethanol or follow the protocol for further dehydration in ethanol and embedding or critical point drying (see common trunk) (Table 1).

For a summary of necessary chemicals and solutions, composition of fluids, see Table 2.

Fixation of liver wedge biopsies (mostly applied to human liver tissue) (Figure 1C)

Wedge biopsies of roughly 1 cm × 1 cm × 1 cm (or less), including the Glisson's capsule at two sides of the wedge, are taken from the margin of a liver lobe as soon as the surgeon/operator has access to the liver. The operator should be cooperative in order to assure that freshness of the tissue is an absolute priority. Directly after opening of the abdomen *via* a chevron incision, the liver is visualized and a wedge is taken with a sharp scissor from the edge of segment 5 or 6, without manipulating the tissue. Bleeding at the biopsy site can easily be controlled using diathermia or argon laser. In a consecutive series of 150 patients no rebleeding at biopsy sites was reported (unpublished results). (1) The tissue is immediately transferred to a 50-mL vessel, filled with PBS (pH 7.4) at 37℃; (2) The tissue is transported to an annex to the operation theater, where injection perfusion with glutaraldehyde fixative is performed in a Petri dish filled with saline; (3) The wedge biopsy is held at a corner by a forceps and is injected by a 25 G syringe from multiple sides with 1.5% glutaraldehyde fixative, until a discoloration and hardening of the tissue, comparable to total liver perfusion, is obtained; (4)

Table 2 Addendum summarizing chemicals necessary for fixation of liver tissue

Compound	Quantity
Cacodylate buffer 0.2 mol/L, pH 7.4	700 mL
Sodium cacodylate trihydrate (Sigma, C0250)	22.9 g
MQ-(purified by ion-exchange)-water	674.8 mL
HCl (0.2 mol/L)	25.2 mL
Filter through 0.2 μm Millipore or Wattman filter paper	
Cacodylate buffer 0.15 mol/L, pH 7.4	
Cacodylate buffer 0.2 mol/L	900 mL
MQ-water	300 mL
Filter through 0.2 μm Millipore or Wattman filter paper	
Glutaraldehyde fixative, 1.5% in cacodylate buffer 0.067 mol/L	
Cacodylate buffer 0.2 mol/L	575 mL
Sucrose (Sigma, S0389)	17.215 g
Glutaraldehyde solution 70% (Sigma, G7776)	36.96 mL
MQ-water	1113.04 mL
Filter	
Osmium tetroxide 1% in phosphate buffer[1]	90 mL (6 × 15 mL)
Osmium tetroxide 4% for EM (Sigma, 75632)	22.5 mL
Phosphate buffer 0.2 mol/L	45 mL
MQ-water	22.5 mL
Washing buffer 1	
Cacodylate buffer 0.2 mol/L	30 mL
Sucrose	0.9 g
MQ-water	60 mL
Washing buffer 2	
Phosphate buffer 0.2 mol/L	45 mL
MQ-water	45 mL
Phosphate buffer 0.2 mol/L pH 7.4 (200 mL)	200 mL
0.2 mol/L $Na_2HPO_4.2H_2O$ (17.8 g in 500 mL MQ-water)	162 mL
0.2 mol/L $NaH_2PO_4.H_2O$ (13.8 g in 500 mL MQ-water)	38 mL

Fluids and chemicals (volumes to be adapted to needs). [1]An alternative to the osmium postfixation is addition of 1.5% potassium ferrocyanide to 1% osmium in veronal acetate buffer (pH 7.4) at 4℃ for 2 h, which strongly enhances the contrast of membranes in cells and tissues[20] (see Figure 13).

Care should be taken that the injection needle does not operate as a biopsy needle; it should be and stay completely filled with glutaraldehyde during injection into the tissue; (5) After injecting the needle into the tissue, parallel to the capsule rim, the needle should be withdrawn a few millimeters before starting injection of the fixative fluid. The idea is to create a space within the tissue in which the fixative can spread out; (6) Injections should be repeated several times until the blood is flushed out of the tissue and the consistency has changed to that of a hard-boiled egg; (7) The time between excision of the wedge and perfusion with fixative is critical. Total glutaraldehyde time (before washing and before osmication) should not exceed 20 min; and (8) After perfusion with glutaraldehyde, the biopsy is rapidly transported to the laboratory, where slices (1 mm thick), strips (1 mm × 1 mm × 5 mm), small flat slices (5 mm × 5 mm × 1 mm) and tissue blocks (1 mm × 1 mm × 1 mm) can be cut under fluid with a clean, sharp razor blade.

Immersion fixation of liver needle biopsies (Figure 1D)

The percutaneous liver biopsy procedure starts with local anesthesia with 1% lidocaine. Under real-time ultrasound guidance, the liver and the biopsy needle are imaged throughout the procedure. The biopsy is taken by a cut-

ting-type needle and a spring-loaded device. A 16-gauge needle is placed into the liver parenchyma before the device is triggered. This results in a liver specimen of 1-2 cm in length, with the diameter being dependent on the size of the biopsy needle (1-1.8 mm). After collecting the biopsy, the fresh tissue is placed in a Petri dish in which 3 mm × 1 mm × 1 mm pieces of the ends of the cylinder are cut. The remaining tissue is used for diagnostic purposes in the pathology department and separately undergoes routine pathology fixation. This procedure should not take longer than 30 s. The two cylinder-shaped tissue pieces of 3 mm × 1 mm are covered with fixative, cut into 1 mm × 1 mm × 1 mm pieces and transferred to a 15-mL vessel that is filled with 1.5% glutaraldehyde fixative at room temperature. The vessel is gently shaken a few times. The total glutaraldehyde time (before washing and osmication) should be no less than 1 h, in order to allow the fixative to penetrate the tissue. After glutaraldehyde, the tissue will be further processed in washing buffer, osmium fixative, and ethanol dehydration.

Fixation of liver cell cultures

The procedure is as follows: (1) cells are cultured on 1 cm diameter glass or plastic coverslips (0.17 mm thick) in wells of culture dishes; (2) cultures are washed three times with 37℃ buffer to rinse away dead cells, cellular debris and precipitates; (3) culture medium is replaced with glutaraldehyde fixative; (4) one should take care that the cells are always covered by a layer of fluid, so that the meniscus does not touch the cells; (5) fluids are changed several times to ensure complete replacement; (6) wash in cacodylate buffer; (7) postfix in 1% osmium tetroxide in phosphate buffer; (8) wash in phosphate buffer; and (9) dehydrate by starting with 70% ethanol (Table 1, Figures 2 and 3).

Critical point drying (CPD) is used routinely to dry samples for SEM[24]. Nation[25] has reported an alternative method that consists of air-drying of insect tissues by rapid evaporation of hexamethyldisilazane (HMDS), which has a very low surface tension. This is supposed to avoid fracturing and destruction of the specimen during drying. In spite of the advantages of HMDS, such as the absence of high pressure equipment, CPD seems to be the most frequently used method. Drying of biological samples by CPD also causes a shrinkage of about 30% of the volume[26]. We have routinely and successfully applied HMDS to cultured liver cells[27]. HMDS drying takes only 3 min instead of the laborious and time-consuming CPD process. We also have applied HMDS drying to perfusion-fixed liver tissue, and during a comparison with CPD, no differences could be seen between the two methods (Figure 3).

After 100% ethanol, samples are immersed for 3 min (cell cultures) or 10 min (liver tissue) in 100% HMDS. After HMDS, the samples are removed from the culture wells and excess HMDS is blotted away by filter paper. The samples are then transferred to a desiccator for 25 min to avoid water contamination. After drying, the samples are mounted on stubs (Figures 4 and 5) and are sputter-coated with 10 nm gold and made available for SEM investigation.

Figure 2 Transmission electron microscopy (TEM) image of an ultrathin section of a plastic-embedded liver sinusoidal endothelial cell after isolation. In the upper part of the picture is a small portion of the nucleus. The labyrinth-like structures in the cytoplasm represent fenestrae that are internalized during the isolation procedure. Electron-dense granules represent lysosomes that reflect the high digestive capacity of these cells. Magnification 6300 ×.

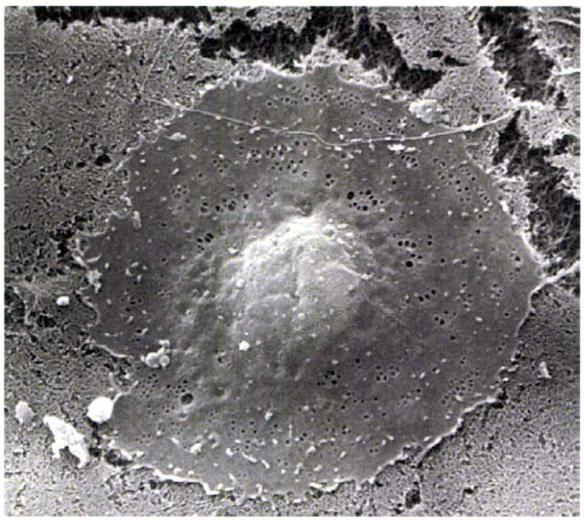

Figure 3 Scanning electron microscopy (SEM) image of a critical-point-dried liver sinusoidal endothelial cell in culture, 2500 ×. After isolation and purification, cells were seeded on a layer of collagen. Besides the centrally located, bulging nucleus, fenestrae can be easily observed in the surrounding thin, flat cytoplasm.

Preparing sections for LM

Follow the instructions given for TEM and make sections of 0.5-1 μm, stain with Toluidine Blue (1% with 2% borate in distilled water), cover sections with Entellan and a 0.17-μm glass coverslip. In case of sufficient contrast, use bright field microscopy, in case of low or insufficient contrast, use phase contrast or interference contrast.